Design and Optimisation of Novel Benzimidazole Hybrid Structures Capable of Simultaneous Peroxisome Proliferator Activated Receptor γ and Angiotensin Receptor Modulation

Submitted in partial fulfilment

of the requirements of the

Degree of Master of Pharmacy

Matthias Borg

Department of Pharmacy

2025

Dedicated to the memory of my beloved grandmother, Maria Antonia, whose wisdom, values and unconditional love continue to guide me in every endeavour I may pursue

Abstract

Metabolic syndrome, associated with an increased risk of diabetes mellitus and cardiovascular disease, is poorly controlled with polypharmacy, prevalent in current management. Dual PPARγ/ATR modulators have potential in metabolic syndrome management. The aims of this study were to use the binding interactions of the benzimidazole scaffold with PPARγ and ATR to model structures with simultaneous high affinity for both loci using virtual screening and *de novo* fragment-based drug design. A consensus pharmacophore was generated in LigandScout® v4.4 by superimposing telmisartan and olmesartan from PDB crystallographic depositions 3VN2 and 4ZUD respectively, together with HTR-04. This pharmacophore was read into ZINCPharmer® with Rule of 3 filters applied. Hits were docked into protomols, describing the energetically unsatisfied space, within the PPARγ and ATR to measure affinity of hits to protomols. In *de novo* fragment-based drug design, two-dimensional topology maps of HTR-04 within the PPARγ and ATR ligand binding pockets guided the generation of seeds derived from HTR-04. Seeds were used for *de novo* growth at predesignated loci within the PPARγ and ATR ligand binding pockets. The study was conducted at the Department of Pharmacy, University of Malta. 519 Lipinski-Rule compliant hits were identified during the virtual screening phase. After docking into protomols, affinity of the 10 highest-ranking hits, expressed as a total score, ranged from 4.28 to 5.08. Using the *de novo* design approach, 4132 molecules were generated from 1 successful seed, of which the top 200 structures were further subjected to filtration for Lipinski Rule compliance. The benzimidazole scaffold shows potential in the development of dual PPARγ/ATR modulators for MetS management. The virtual screening and *de novo* design approaches both identified high-affinity drug candidate molecules suitable for further optimisation.

Acknowledgments

I would like to express my deepest gratitude to my dissertation supervisor, Dr. Claire Shoemake, for her invaluable guidance, patience, and encouragement throughout the course of this research. Her expertise and support have been instrumental in shaping this work.

My sincere thanks also go to Prof. Lilian M. Azzopardi & the Department of Pharmacy at the University of Malta for providing me with the knowledge, resources, and academic environment necessary throughout these past five years. I am especially grateful to all my lecturers and mentors within the department, whose dedication and teaching have greatly inspired me.

I am indebted to my family for their unconditional love, understanding, and unwavering support. Their encouragement and belief in me have been a constant source of strength throughout this journey.

To my university classmates, I extend heartfelt thanks for their camaraderie, collaboration, and shared experiences. The discussions, advice, and moments of laughter made this path more rewarding.

Finally, I would like to thank the staff at Joyce's Pharmacy for their support, kindness, and flexibility during my studies. Their encouragement and practical insights have not only enriched this thesis but also my growth as a professional.

To all who contributed in any way to the completion of this work, I am truly grateful.

Table of Contents

List of Tables

List of Figures

List of Abbreviations

2D	Two-Dimensional
3D	Three-Dimensional
ADME	Absorption, Distribution, Metabolism and Elimination
AR	Aromatic Ring
ARB	Angiotensin II Receptor Blocker
ATR	Angiotensin II Receptor
BP	Blood Pressure
CADD	Computer-Aided Drug Design
CLogP	Calculated Log P
CVD	Cardiovascular Disease
FBDD	Fragment-Based Drug Design
FIP	International Pharmacy Federation
FREC	Faculty Research Ethics Committee
GLP-1RA	Glucagon-like Peptide 1 Receptor Agonist
HBA	Hydrogen Bond Acceptor
HBD	Hydrogen Bond Donor
HI	Hydrophopic Interactions
IP	Inositol Phosphate
LBA	Ligand Binding Affinity

LBDD	Ligand-Based Drug Design
LBP	Ligand-Binding Pocket
LD_{50}	Lethal Dose 50
LDL-C	Low-Density Lipoprotein Cholesterol
MD	Molecular Dynamics
MetS	Metabolic Syndrome
MHRA	Medicines and Healthcare products Regulatory Agency
MW	Molecular Weight
PDB	Protein Data Bank
pKd	Dissociation Constant
PPAR	Peroxisome Proliferator Activated Receptor
RCSB	Research Collaboratory for Structural Bioinformatics
SBDD	Structure-Based Drug Design
SMILES	Simplified Molecular Input Line Entry System
SPPARγM	Selective PPARγ Modulator
SRC1	Steroid Receptor Coactivator-1
T2DM	Type 2 Diabetes Mellitus
VMD	Visual Molecular Dynamics
VS	Virtual Screening
XBD	Halogen Bond Donor

Chapter 1

Introduction

1.1 Metabolic Syndrome

Metabolic syndrome (MetS) first identified in the early 1900s, has seen a surge in prevalence due to rising rates of obesity and type 2 diabetes mellitus (T2DM), prominent characteristics of the syndrome. MetS is a common clinical condition, particularly in the Western world, where sedentary lifestyles, poor eating habits and obesity are prevalent (Pérez-Martínez *et al.*, 2017). In the US, over 40% of individuals aged over 60 are affected (Cross & Underwood, 2019) by MetS. The syndrome encompasses a number of conditions including central obesity, hyperglycaemia, hypertriglyceridemia, hypertension and low levels of high-density lipoprotein cholesterol levels (O'Toole, 2017; Cross & Underwood, 2019). MetS has serious clinical implications, and is linked to increased predisposition to T2DM and cardiovascular disease (CVD) (O'Toole, 2017). CVD is a leading global cause of death, one which imposes a substantial economic burden (Kokubo *et al.*, 2008; Mottillo *et al.*, 2010) and is associated with increasing medical expenditure (Choo *et al.*, 2016). Evidence shows that MetS increases cardiovascular risk beyond that attributable to its individual risk factors (Gami *et al.*, 2007) contributing to a 1.5-fold increase in overall mortality and a 2-fold increase in cardiovascular comorbidities (Mottillo *et al.*, 2010).

The present pharmacological options mostly target individual components of MetS to minimise or prevent CVD and T2DM. Polypharmacy, a growing issue prevalent among patients with MetS (Grant *et al.*, 2003; Noale *et al.*, 2016; Alwhaibi *et al.*, 2018) demonstrates only modest effectiveness (Wang *et al.*, 2020). No approved medicines that can reliably control MetS over the long-term are currently available (Grundy *et al.*, 2005; Grundy, 2006; Handelsman & Jellinger; 2011; Peterseim *et al.*, 2024). A single drug with multiple actions to control MetS is a potential solution to polypharmacy (Rollason & Vogt, 2003; Lillich *et al.*, 2021). Dual peroxisome proliferator-activated receptor (PPAR)

γ agonists that also antagonise angiotensin II receptor (ATR) subtype 1, are often considered as a suitable target combination for the treatment of MetS (Lillich *et al.*, 2021; Lin & Sun, 2024). The antihypertensive drug, telmisartan was the first dual PPARγ/ATR ligand identified (Ries *et al.*, 1993; Benson *et al.*, 2004) and ongoing research being conducted aims to enhance PPARγ modulation while maintaining ATR antagonism of telmisartan (Lillich *et al.*, 2021).

1.2 Current Management of MetS

Visceral obesity reduction, glucometabolic homeostasis improvement, blood pressure (BP) control and hypertriglyceridemia management can be achieved through weight reduction strategies (Rigamonti *et al.*, 2021). First-line pharmacological recommendations include statins for dyslipidaemia, renin-angiotensin-aldosterone system inhibitors for hypertension, metformin, sulfonylureas, dipeptidyl peptidase-4 inhibitors, sodium-glucose cotransporter-2 inhibitors and glucagon-like peptide 1 receptor agonists (GLP-1RAs) for glucose intolerance, and GLP-1RAs for body weight and waist circumference (Rask Larsen *et al.*, 2018). Polypharmacy is prevalent in current management of MetS with up to 60% of patients over 65 years old with T2DM being prescribed at least five medications (Noale *et al.*, 2016; Alwhaibi *et al.*, 2018). Polypharmacy increases the risk of adverse drug reactions (Nguyen *et al.*, 2006; Viktil *et al.*, 2007), drug–drug interactions (Rodrigues & De Oliveira, 2016) and therapy duplication (Golchin *et al.*, 2015). Polypharmacy is also associated with decreased medication compliance (Bailey & Kodack, 2011), and suboptimal disease management (Willey *et al.*, 2006). Drug-associated side effects also contribute to poor patient adherence (Grant *et al.*, 2003). Effective anti-diabetic drugs such as PPARγ agonists are associated with reduced compliance and clinical use due to oedema caused by

thiazolidinedione PPARγ agonists namely, rosiglitazone and pioglitazone (Guan *et al.*, 2005; Stafylas *et al.*, 2009). Recent safety concerns have contributed to the late-stage development failure of several PPAR agonists, including newly developed compounds that specifically target PPARγ. These safety issues are diverse and significant, encompassing findings such as a potential carcinogenic effect observed in rodent studies, as well as signs suggestive of muscle toxicity, including myopathy and rhabdomyolysis (Layne *et al.*, 2004). Additional concerns include possible impairment of renal and metabolic function manifested as elevations in plasma creatinine (Attridge *et al.*, 2013) and homocysteine levels, respectively (Taskinen *et al.*, 2009). These compounds have also been associated with undesirable effects such as weight gain, fluid retention, haemodilution and peripheral oedema leading to increased risks of heart failure, limiting the therapeutic viability of these agents (Nesto *et al.*, 2005, Nissen *et al.*, 2005). Research has shown that prescription of pharmacotherapy for all individual components of MetS appears to be substantially insufficient and unsuccessful (Rigamonti *et al.*, 2021). Treatment that targets more than one cardiovascular risk factor such as lowering of BP, decreasing low-density lipoprotein cholesterol (LDL-C) and lowering blood glucose levels would greatly improve patient adherence, simplify treatment regimens, and enhance outcomes (Handelsman & Jellinger, 2011). Development of such medications could potentially optimise MetS management (Lillich *et al.*, 2021).

1.3 Novel Approach

Novel and safer natural PPARγ agonists have garnered significant interest as potential management options for MetS (Alam *et al.*, 2021). Pioglitazone, a synthetic PPARγ agonist used in treating T2DM (Abbas *et al.*, 2012), has demonstrated efficacy in reducing or preventing hypertension (Usuda, 2014) in both animal (Dovinová *et al.*, 2013) and

human (Abe *et al.*, 2008) models. Activation of PPAR in the rostral ventrolateral medulla, a critical brain area involved in cardiovascular control, reduced angiotensin II-induced hypertension in rats (Chan *et al.*, 2009; Yu *et al.*, 2015). Telmisartan, an angiotensin II receptor blocker (ARB), has a unique central benzimidazole and propyl group that can occupy a narrow hydrophobic pocket in the PPARγ that other ARBs cannot occupy effectively. These structural properties allow telmisartan to interact with PPARγ and support its activation with a similar conformational change and coregulator profile as thiazolidinediones (Schupp *et al.*, 2005). This property could mitigate adverse effects of thiazolidinediones and other PPARγ agonists (Shindo *et al.*, 2012; Kolli *et al.*, 2014; Wang *et al.*, 2014). Telmisartan has been identified as a selective PPARγ modulator (SPPARγM) and is a bifunctional ligand, functioning as both an ARB and a partial PPARγ agonist (Imayama *et al.*, 2006; Gao *et al.*, 2018; Bernardo *et al.*, 2021; Wang *et al.*, 2022). Clinical trials were conducted to confirm the benefits of telmisartan on glucose and lipid metabolism when compared to other ARBs, however the results were varied (Derosa *et al.*, 2004; Vitale *et al.*, 2005; Hamada *et al.*, 2014; Naruse *et al.*, 2019). A meta-analysis of randomised controlled studies found that telmisartan was superior in improving insulin resistance, lowering fasting blood glucose and blood insulin levels (Wang *et al.*, 2018).

The difference in effective telmisartan concentrations for pharmacodynamic modulation of the PPARγ and ATR receptors is significant. Research has been conducted to develop more effective PPARγ modulators while maintaining ATR receptor antagonism of telmisartan (Lillich *et al.*, 2021).

1.3.1 Multi-Target Therapeutics

Rational multi-target drug design approaches consist of small molecules directed at two or more endogenous targets. In the development of multi-target therapeutics, appropriate target combinations must be selected. Synergistic combinations are also favourable, enhancing the safety and efficacy of the therapeutic agent as exemplified in oncology and infectious disease (Lillich *et al.*, 2021). Dual PPARγ/ATR modulators are amongst the most notable multi-target therapeutics for metabolic conditions such as MetS, where synergistic multi-drug targets are not yet well-established (Proschak *et al.*, 2019). Through this research, dual PPARγ/ATR modulators for the management of MetS can be designed. Successful drug design at the PPARγ and ATR *loci* can address the needs of the current management of MetS to improve clinical outcomes and decrease the issues associated with polypharmacy, prevalent in current management of MetS.

1.4 The Benzimidazole Scaffold

Benzimidazoles have revolutionised medicinal chemistry due to their numerous biological activities, with a number of drugs including telmisartan containing the benzimidazole scaffold (Yadav & Ganguly, 2015). Structural modifications of benzimidazoles have also been shown to have therapeutic potential as antidiabetic agents (Kwak *et al.*, 2013). A better understanding of the structural, physical and chemical properties of benzimidazoles may aid researchers to employ this structure in the pharmacological management of inadequately controlled diseases. Serious side effects associated with the benzimidazoles can also be identified and addressed (Yadav & Ganguly, 2015).

1.5 PPARγ Partial Activation

Telmisartan functions as a partial agonist of the nuclear receptor PPARγ. In a high-resolution (2.18 Å) crystallographic study, Amano *et al.* (2012) elucidated the ternary complex comprising PPARγ, telmisartan, and a steroid receptor coactivator-1 (SRC1) peptide (as depicted in Figure 2.2). The analysis revealed that telmisartan adopts a U-shaped conformation positioning its central benzimidazole ring within branch I of the PPARγ ligand-binding pocket (LBP). This binding configuration displaces the His^{323} residue and disrupts the canonical hydrogen-bonding network characteristic of full agonists (Amano *et al.*, 2012).

Unlike full agonists, which typically establish three to four stabilising hydrogen bonds, telmisartan engages in only a single critical hydrogen bond with Tyr^{473}. This attenuated hydrogen-bond network around helix 12 reduces coactivator peptide recruitment, mediating partial rather than full receptor activation (Amano *et al.*, 2012). The agonistic activity of telmisartan is instead supported predominantly by hydrophobic interactions within other branches of the LBP. Owing to its dual pharmacological profile as both a potent ARB and a SPPARγM, telmisartan presents therapeutic promise for the management of hypertension, CVD, and metabolic disorders such as T2DM, with the potential for fewer adverse effects compared to full PPARγ agonists such as the thiazolidinediones (Amano *et al.*, 2012).

1.6 ATR Antagonism

The ATR plays a central role in BP regulation. ARBs are extensively employed in clinical practice as antihypertensive agents for the management of hypertension, diabetic nephropathy, cardiac hypertrophy, and renal failure (Imaizumi *et al.*, 2013). ARBs

generally possess a common chemical scaffold. Subtle structural modifications can result in markedly different therapeutic outcomes in the management of CVD. While the majority of ARBs are classified as neutral antagonists of the ATR, olmesartan serves as an exception, functioning as an inverse agonist with respect to inositol phosphate (IP) production (Miura *et al.*, 2006).

An X-ray crystallographic study carried out by Zhang *et al.* (2015) that elucidated human ATR in complex with inverse agonist olmesartan at a high resolution of 2.8 Å (as depicted in Figure 2.3) revealed that ARBs with conserved structural scaffolds engage overlapping molecular recognition sites on the ATR. Three residues, Arg^{167}, Trp^{84}, and Tyr^{35}, were noted to be essential for the binding of most ARBs, forming extensive interactions with the ligand. In certain cases, ARB binding involves further interactions with ATR sub-pockets. Chemical modifications to the common biphenyl-tetrazole scaffold in olmesartan-derived compounds confer distinct functional selectivity, yielding pharmacological profiles that span from inverse agonism to antagonism to partial agonism (Zhang *et al.*, 2015).

1.7 Rational Drug Design

Rational drug design describes the multi-dimensional optimisation of the physicochemical, absorption, distribution, metabolism and elimination (ADME) and toxicological profiles of a drug molecule to satisfy the predefined pharmacological efficacy (Davis *et al.*, 2003). The three-dimensional (3D) structure of proteins and protein-ligand complexes is determined using techniques including nuclear magnetic resonance (NMR) spectroscopy and X-ray crystallography (Wüthrich, 2001; Blundell *et al.*, 2002). The role of rational drug design is indispensable in modern drug discovery

(Swinney & Anthony, 2011). As structural information becomes more relevant in drug discovery, the limitations of experimentally determined structures must be identified to avoid the consequences of misusing structural information. A successful rational drug design approach involves selecting suitable structures from the start and acknowledging the inherent flexibility of proteins (Sun, 2016). The ultimate aim of rational drug design is to identify and design small molecules that are sterically and electrostatically complementary to their targets, allowing the ligands to bind strongly to these targets and regulate their biological functions (Sun, 2016).

1.8 Computer-Aided Drug Design Tools & Software

Computer-aided drug design (CADD) encompasses a number of computational methodologies aimed at facilitating and accelerating the drug discovery process. These methodologies involve the systematic identification of relevant biological targets, the virtual screening (VS) of extensive chemical libraries, the structural optimisation of lead compounds, and the preliminary assessment of toxicity profiles through *in silico* modelling and web-based laboratories (Sliwoski *et al.*, 2013; Yang *et al.*, 2019). By integrating these computational approaches, the number of chemical entities requiring experimental validation can be substantially reduced. This strategy enables the prioritisation of molecules with the highest likelihood of therapeutic efficacy and safety, mitigating the scale, duration, and financial burden typically associated with conventional experimental drug discovery workflows (Sliwoski *et al.*, 2013; Yang *et al.*, 2019; Wu *et al.*, 2024).

CADD is comprised of structure-based drug design (SBDD) and ligand-based drug design (LBDD). SBDD approaches incorporate techniques such as molecular docking,

molecular dynamics (MD) simulations, and *de novo* drug design, all of which leverage structural information about the target macromolecule to guide compound development (Wu *et al.*, 2024). LBDD methodologies rely on knowledge of the physicochemical and biological properties of known ligands and include strategies such as quantitative structure–activity relationship modelling, pharmacophore modelling and similarity-based VS (Wu *et al.*, 2024). Fragment-based drug design (FBDD) involves the identification of chemical fragments of low molecular weight (MW) with binding affinity to the target, followed by their systematic optimisation through fragment growing or fragment linking techniques (Wang *et al.*, 2023). Owing to their inherently low MW, fragment hits typically exhibit weak binding affinity toward their target macromolecules. These initial fragments must undergo systematic elaboration into larger, more complex structures with enhanced binding properties to be made into viable lead compounds (Kirsch *et al.*, 2019). FBDD has emerged as a powerful approach in this context, enabling a comparatively high success rate in the identification of leads, while simultaneously accelerating the overall development timeline and reducing the financial burden associated with conventional drug discovery strategies (Kirsch *et al.*, 2019). The early stages of fragment growth and optimisation towards molecules with improved biological activity can often proceed without the need for direct intervention from medicinal chemists, streamlining the initial phases of the drug discovery process and allowing for a more efficient transition from molecular fragments to potent lead compounds (Zhou *et al.*, 2021; de Oliveira *et al.*, 2023).

1.8.1 BIOVIA Discovery Studio Visualizer® v24.1

BIOVIA Discovery Studio Visualizer® is a platform designed for the visualisation and analysis of molecular docking results, facilitating the interpretation of ligand–protein

interactions. Its key visualisation capabilities include 3D molecular structure viewing, ligand–protein interaction exploration and complex visualisation, supplemented by two-dimensional (2D) interaction diagrams (Baroroh *et al.*, 2023). The software provides tools for identifying hydrogen bonds, hydrophobic interactions, and other non-bonded interactions, alongside features for assessing binding affinity and complex stability (Baroroh *et al.*, 2023).

1.8.2 SYBYL-X® v1.1

SYBYL-X® offers a comprehensive suite of tools for the construction, visualisation, and analysis of both macromolecular and small molecule structures. SYBYL-X® functionalities encompass molecular model building, structural superimposition, geometry optimisation, and distance geometry calculations (Ash *et al.*, 2010). The SYBYL-X® platform supports molecular docking studies and provides interfaces to quantum mechanical calculations as well as other advanced computational methodologies, thereby enabling a wide range of applications in molecular modelling and drug design (Ash *et al.*, 2010).

1.8.3 LigandScout® v4.4

LigandScout is a computational tool designed to generate 3D pharmacophore models from structural data of ligand-protein complexes. It defines 3D spatial arrangements of chemical features such as hydrogen bond donors and acceptors, lipophilic regions, and ionisable groups that characterise ligand–protein interactions (Wolber & Langer, 2005). Using a pattern-matching alignment algorithm based on pharmacophoric feature points, multiple pharmacophores can be overlaid to identify common interactions and derive

shared-feature pharmacophores. These pharmacophores are then utilised in the *in silico* screening of large compound databases (Wolber & Langer, 2005).

1.8.4 ZINCPharmer®

ZINCPharmer® is a web-based platform that facilitates the search of purchasable compounds within the ZINC database through the Pharmer pharmacophore search engine. The platform allows users screen approximately 176 million conformers representing 18.3 million compounds in under one minute (Koes & Camacho, 2012) . Search results can be viewed immediately online or downloaded for offline analysis, further filtration and molecular docking, enabling fast and interactive exploration of commercially available chemical databases (Koes & Camacho, 2012).

1.8.5 MONA®

MONA® cheminformatics tool designed for the interactive exploration and management of large compound libraries, accessible without complex database setups or specialist expertise. It offers chemically precise handling of molecular structures and enables rapid filtering, clustering, and structural comparison (Hilbig & Rarey, 2015). By allowing flexible organization and analysis of datasets containing up to millions of compounds, MONA® streamlines key tasks in drug design such as library curation (by identifying duplicates and resolving tautomers), compound selection, and post-processing of screening results. Its efficiency, ease of use, and ability to integrate diverse chemical data sources make it a valuable resource for accelerating early-stage drug discovery workflows (Hilbig & Rarey, 2015).

1.8.6 X-SCORE® v1.3

X-SCORE® is a computational scoring function developed to quantitatively evaluate the binding affinity of protein-ligand complexes with known 3D structures and comparing protein–ligand interactions *in silico* (Wang *et al.*, 2002). By analysing structural and energetic features derived from 3D coordinates, X-SCORE® estimates the binding free energy, particularly valuable in SBDD and FBDD, where accurate prediction of binding affinities can guide lead optimisation, prioritise candidate molecules, and improve the efficiency of VS and *de novo* workflows (Wang *et al.*, 2002).

1.8.7 LigBuilder® v1.2

LigBuilder® is the pioneering software for *de novo* multi-target drug design, enabling the creation of ligands that can interact with multiple receptors, different binding sites within the same receptor, or different receptor conformations (Yuan *et al.*, 2020). LigBuilder® is broadly applicable for designing and optimising multi-target drugs and exploring diverse ligand-protein interactions (Yuan *et al.*, 2020).

1.8.8 Visual Molecular Dynamics® v1.9.3

Visual Molecular Dynamics (VMD) is a molecular visualisation tool used for displaying and analysing molecular assemblies including proteins and small molecules. VMD® supports the simultaneous visualisation of multiple structures, offering a range of rendering styles (Humphrey *et al.*, 1996).

1.8.9 ProTox 3.0®

ProTox 3.0® is an open-access computational platform developed for the *in silico* prediction of chemical toxicity. ProTox 3.0® integrates molecular similarity, fragment-based modelling, and advanced machine learning techniques to evaluate 61 toxicity endpoints, including acute oral toxicity, organ-specific effects, mutagenicity, carcinogenicity, and metabolism-related toxicities (Banerjee *et al.*, 2024). By allowing users to input chemical structures, the platform generates comprehensive toxicity profiles with confidence scores. ProTox 3.0® provides a rapid alternative to conventional animal-based testing, aligning with green toxicology principles by reducing reliance on *in vivo* methods (Maertens *et al.*, 2014). ProTox 3.0® is widely applied in drug discovery, environmental risk assessment and regulatory decision-making, where early and cost-effective toxicity evaluation is essential (Banerjee *et al.*, 2024).

1.9 Aim

The aim of this research project was to use the binding interactions of the benzimidazole scaffold with both PPARγ and ATR receptors to model structures with simultaneous high affinity for both *loci* using VS and *de novo* FBDD techniques.

Chapter 2

Methodology

2.1 Ethics Approval

This research project was acknowledged by the Faculty Research Ethics Committee (FREC) of the faculty of Medicine & Surgery under the Application ID MED-2024-00115 (Appendix 1). The application was submitted for records purposes.

2.2 Literature Review

A literature review was undertaken to obtain background information on the current management of MetS, identify lead molecules and understand the roles of PPARγ and ATR in the MetS. The literature review aimed to identify *lacunae* in the current pharmacological management of MetS and novel approaches that can target more than one cardiovascular risk factor associated with MetS whilst improving clinical outcomes and patient adherence to therapy. Articles reviewed were free full-text articles published in English by peer-reviewed journals obtained from the online databases PubMed®, ProQuest®, Google Scholar®, and HyDi. Other publications utilised included the Research Collaboratory for Structural Bioinformatics (RCSB) Protein Data Bank (PDB) website. The RCSB PDB is the US data centre for the global PDB archive of 3D structure data for large biological molecules including proteins, DNA, and RNA (Bernstein *et al.*, 1977).

2.3 Selecting PDB Crystallographic Depositions 3VN2 & 4ZUD & Hybrid Benzimidazole Structures

A series of benzimidazole structures, HTR-01, HTR-02, HTR-03 and HTR-04 were identified in a study by Chittiboyina *et al.*, 2009 (Figure 2.1). Of these hybrid benzimidazoles, HTR-04 was found to be more active than HTR-01 and HTR-02 and

bulky groups at the R_1 position for HTR-03 were not well tolerated for ATR activity (Chittiboyina *et al.*, 2009). Based on these findings, HTR-04 was chosen as the lead molecule for this study and was modelled in SYBYL-X® v1.1 (Ash *et al.*, 2010). 195 structures describing human PPARγ were identified from the RCSB PDB of which PDB crystallographic deposition 3VN2[1] describing the bound coordinates of human PPARγ in complex with ATR antagonist and partial PPARγ agonist, telmisartan (Zhang *et al.*, 2007; Amano *et al.*, 2012; Tan *et al.*, 2012) was selected. 10,624 PDB structures describing ATR were also identified, of which 4835 structures described human ATR. 4ZUD[2] describing the bound coordinates of human ATR in complex with inverse agonist olmesartan was selected. Both PDB structures were resolved using X-ray crystallography with PDB crystallographic deposition 3VN2[1] being resolved at 2.18Å while PDB crystallographic deposition 4ZUD[2] was resolved at 2.80Å.

[1] Amano Y. RCSB PDB - 3VN2: Crystal structure of PPARgamma complexed with telmisartan [Internet]. United States: RCSB PDB. 2012 [cited 2025 Jul 4]. Available from: https://www.rcsb.org/structure/3VN2.
[2] Zhang H, Unal H, Desnoyer R, Han GW, Patel N, Katritch V, *et al.* RCSB PDB - 4ZUD: Crystal structure of human angiotensin receptor in complex with inverse agonist olmesartan at 2.8Å resolution. [Internet]. United States: RCSB PDB. 2015 [cited 2025 Jul 4]. Available from: https://www.rcsb.org/structure/4ZUD.

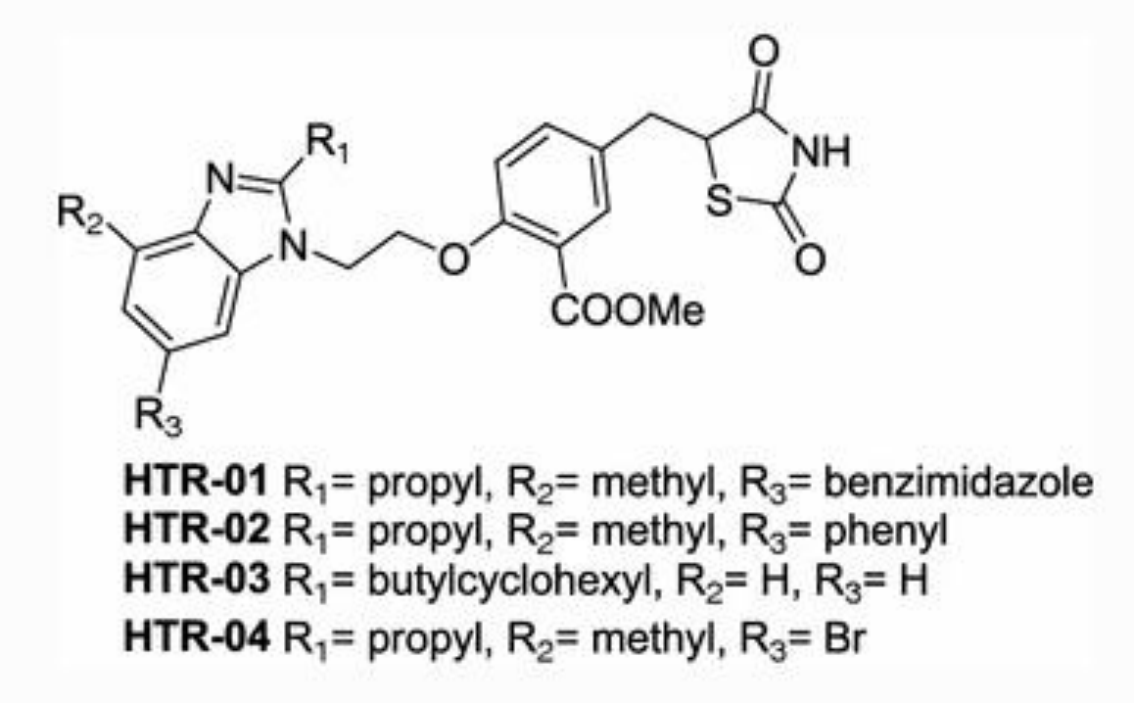

Figure 2.1: Hybrid benzimidazoles HTR-01, HTR-02, HTR-03, and HTR-04. Reproduced from: Chittiboyina AG, Mizuno CS, Desai PV, Patny A, Kurtz TW, Pershadsingh HA, *et al.* Design, synthesis, and docking studies of novel telmisartan–glitazone hybrid analogs for the treatment of metabolic syndrome. Medicinal Chemistry Research. 2009;18(7):589–610.

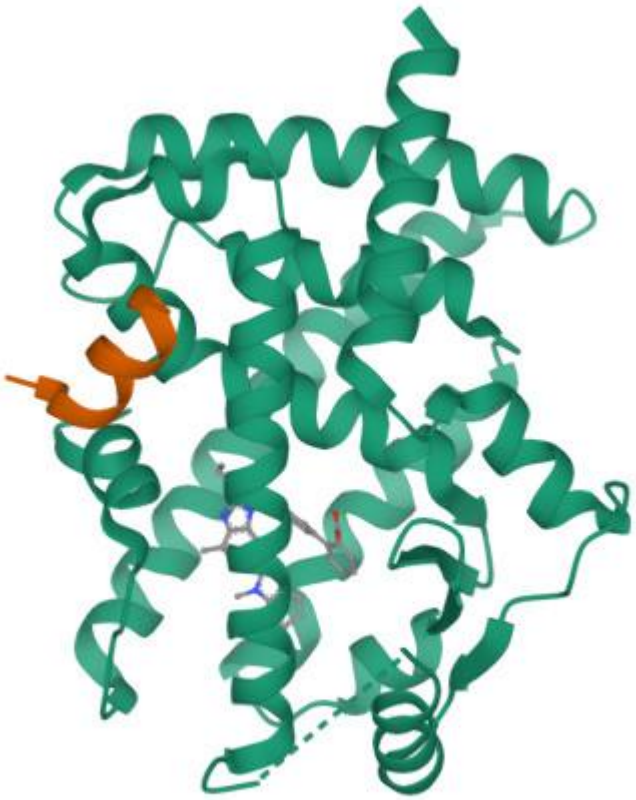

Figure 2.2: PDB crystallographic deposition 3VN2 describing the bound coordinates of human PPARγ in complex with partial agonist telmisartan at a resolution of 2.18Å.[1]

[1] Amano Y. RCSB PDB - 3VN2: Crystal structure of PPARgamma complexed with telmisartan [Internet]. United States: RCSB PDB. 2012 [cited 2025 Jul 4]. Available from: https://www.rcsb.org/structure/3VN2.

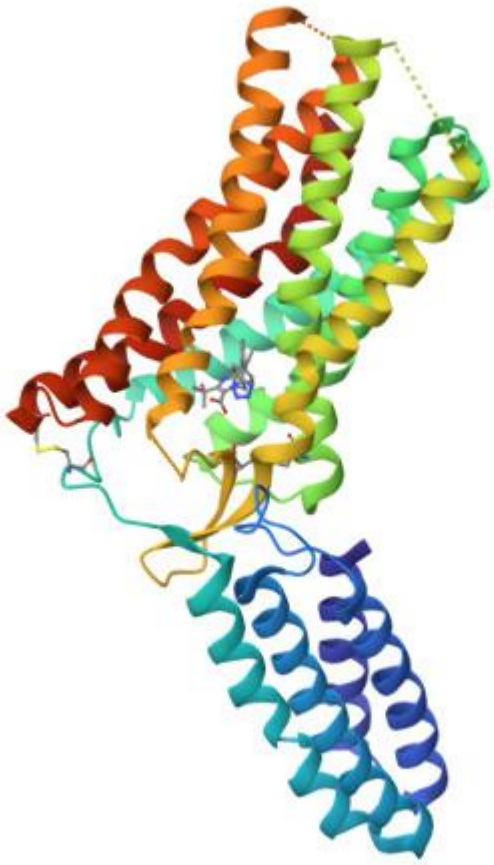

Figure 2.3: PDB crystallographic deposition 4ZUD describing the bound coordinates of human ATR in complex with inverse agonist olmesartan at a resolution of 2.80Å.[2]

2.4 Virtual Screening

VS is a computer-aided technique used in drug discovery to identify potential drug candidates by evaluating large libraries of chemical compounds (Wu *et al.*, 2024). This process involves using computational models to analyse and predict which of these compounds are most likely to interact effectively with specific target receptor proteins,

[2] Zhang H, Unal H, Desnoyer R, Han GW, Patel N, Katritch V, *et al.* RCSB PDB - 4ZUD: Crystal structure of human angiotensin receptor in complex with inverse agonist olmesartan at 2.8Å resolution. [Internet]. United States: RCSB PDB. 2015 [cited 2025 Jul 4]. Available from: https://www.rcsb.org/structure/4ZUD.

thereby enabling the ranking and prioritisation molecules for further experimental testing as potential therapeutic agents (Wu *et al.*, 2024).

VS is designed to efficiently select a subset of promising compounds from extensive chemical libraries by filtering out structurally irrelevant or unsuitable molecules. This strategic narrowing of options significantly reduces the need for excessive experimental resources and laborious procedures. VS serves as a highly valuable step during the early stages of drug discovery. It has gained recognition as a powerful and cost-effective alternative to traditional high-throughput screening methods, increasing the likelihood of identifying biologically relevant compounds, accelerating the discovery process and enhancing the chances of success when dealing with large virtual databases (de Oliveira *et al.*, 2023).

PDB crystallographic depositions 3VN2[1], 4ZUD[2], and the hybrid benzimidazole structure molecule HTR-04 (Chittiboyina *et al.*, 2009) were read into LigandScout® v4.4 (Wolber & Langer, 2005) and pharmacophoric structures were generated and interpreted according to the key in Table 3.1.

2.4.1 Telmisartan Pharmacophore

PDB crystallographic deposition 3VN2[1] was read into LigandScout® v4.4 (Wolber & Langer, 2005) to create a pharmacophore describing the critical contacts of telmisartan with PPARγ. The bioactive conformation of unbound telmisartan was isolated and the critical interactions formed between telmisartan and the amino acids within the LBP of

[1] Amano Y. RCSB PDB - 3VN2: Crystal structure of PPARgamma complexed with telmisartan [Internet]. United States: RCSB PDB. 2012 [cited 2025 Jul 4]. Available from: https://www.rcsb.org/structure/3VN2.
[2] Zhang H, Unal H, Desnoyer R, Han GW, Patel N, Katritch V, *et al.* RCSB PDB - 4ZUD: Crystal structure of human angiotensin receptor in complex with inverse agonist olmesartan at 2.8Å resolution. [Internet]. United States: RCSB PDB. 2015 [cited 2025 Jul 4]. Available from: https://www.rcsb.org/structure/4ZUD.

PPARγ were identified. The pharmacophore generated (Figure 3.3) was superimposed onto the bioactive conformation of unbound telmisartan as depicted in Figure 3.4. A 2D map of the bioactive conformation of telmisartan describing the critical contacts of the telmisartan molecule with the amino acids with the LBP of PPARγ was also rendered in LigandScout® v4.4 (Wolber & Langer, 2005) (Figure 3.5).

2.4.2 Olmesartan Pharmacophore

PDB crystallographic deposition 4ZUD[2] was also read into LigandScout® v4.4 (Wolber & Langer, 2005) creating a pharmacophore describing the critical contacts of inverse agonist olmesartan with ATR as depicted in Figure 3.7. The bioactive conformation of unbound olmesartan was also isolated and the critical interactions formed by olmesartan within the LBP of ATR were also identified. The pharmacophore generated (Figure 3.8) was also superimposed onto the bioactive conformation of unbound olmesartan as depicted in Figure 3.9 and 2D map of the bioactive conformation of olmesartan describing the critical contacts of olmesartan within the LBP of ATR was also rendered in LigandScout® v4.4 (Wolber & Langer, 2005) (Figure 3.10).

[2] Zhang H, Unal H, Desnoyer R, Han GW, Patel N, Katritch V, *et al.* RCSB PDB - 4ZUD: Crystal structure of human angiotensin receptor in complex with inverse agonist olmesartan at 2.8Å resolution. [Internet]. United States: RCSB PDB. 2015 [cited 2025 Jul 4]. Available from: https://www.rcsb.org/structure/4ZUD.

2.4.3 HTR-04 Pharmacophore

The hybrid benzimidazole structure HTR-04 (Figure 2.14) (Chittiboyina *et al.*, 2009) was also read into LigandScout® v4.4 (Wolber & Langer, 2005) as a *.mol2* file and the binding interactions of the modelled structure was used to build a pharmacophoric structure describing the critical contacts of HTR-04 (Chittiboyina *et al.*, 2009) with PPARγ in LigandScout® v4.4 (Wolber & Langer, 2005). The pharmacophore generated (Figure 3.12) was superimposed unbound HTR-04 as depicted in Figure 3.13. The critical interactions formed between hybrid benzimidazole HTR-04 and the amino acids within the LBP of PPARγ were identified.

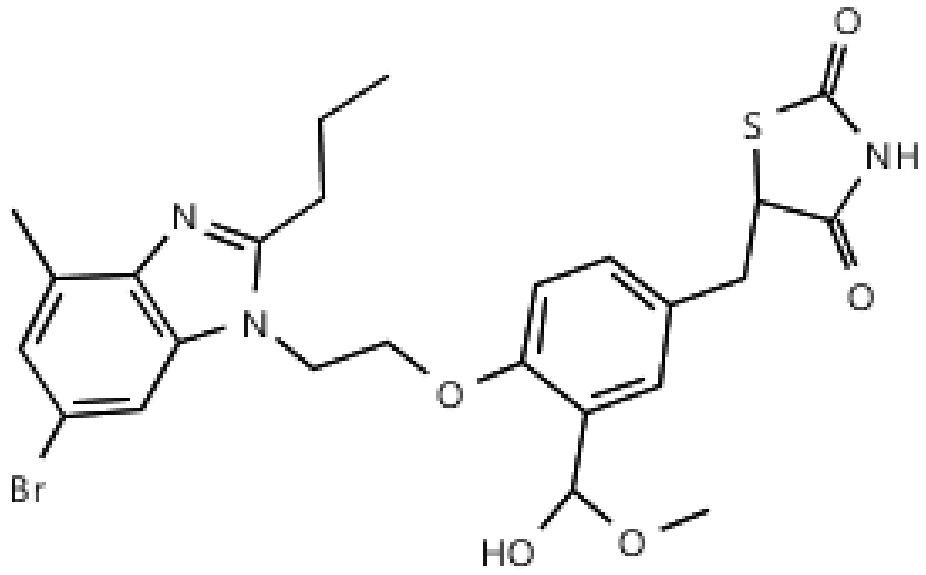

Figure 2.4: 2D structure of the hybrid benzimidazole structure HTR-04 (Chittiboyina *et al.*, 2009).

Reproduced from: Chittiboyina AG, Mizuno CS, Desai PV, Patny A, Kurtz TW, Pershadsingh HA, *et al.* Design, synthesis, and docking studies of novel telmisartan–glitazone hybrid analogs for the treatment of metabolic syndrome. Medicinal Chemistry Research. 2009;18(7):589–610.

2.4.4 Generation of Shared-Feature Pharmacophore

The pharmacophores generated describing the critical contacts of telmisartan molecule with the LBP of the PPARγ, the critical contacts of the inverse ATR agonist olmesartan with the LBP of the ATR, and the critical contacts of hybrid benzimidazole HTR-04 (Chittiboyina *et al.*, 2009) with the LBP of the PPARγ were all superimposed in LigandScout®, generating a shared-feature (or consensus) pharmacophore depicted in Figure 3.14. This shared-feature pharmacophore was exported to ZINCPharmer® database in the screening process for hit molecules (Koes & Camacho, 2012).

2.4.5 Screening for Hits in ZINCPharmer®

The ZINCPharmer® database (Koes & Camacho, 2012) was queried for molecules with similar spatial arrangements and electronic properties as the shared-feature pharmacophore, also referred to as hit molecules using the shared-feature pharmacophore obtained in LigandScout® v4.4 (Wolber & Langer, 2005). Conservative filters in adherence to the Rule of 3 (Congreve *et al.*, 2003) were applied to obtain lead-like hits which remain Lipinski rule compliant after the addition of structural moieties during the process of lead optimisation, safeguarding oral bioavailability. The filters that were applied when querying the ZINCPharmer® database (Koes & Camacho, 2012) are tabulated in Table 2.1.

Table: 2.1: Filters applied in ZINCPharmer® (Koes & Camacho, 2012) when database was queried for hit molecules using the shared-feature pharmacophore generated.

Maximum Hits per Configuration	1
Maximum Hits per Molecule	1
Maximum Total Hits	300
Maximum Root-Mean-Square Deviation (RMSD)	1
MW (Da)	1 – 300
Rotatable bonds	1-3

Hits obtained were exported and saved as structure-data files in *.sdf* format and categorised according to the database from which they were obtained. These databases were ZINC Purchasable, ZINC Purchasable Thiols, ZINC Drug Database, ZINC in Man, ZINC Drug Database (Metabolites), ZINC Natural Derivatives, and ZINC Natural Products.

2.4.6 Protomol Generation

SYBYL-X® v1.1 (Ash *et al.*, 2010) was utilised to generate two protomols for the PDB crystallographic depositions used for this project (3VN2[1] and 4ZUD[2]) and depicted in Figures 3.15 & 3.16 respectively. The holo-complexes 3VN2[1] describing the bound co-ordinates of telmisartan with PPARγ, and 4ZUD[2] describing the bound co-ordinates of

[1] Amano Y. RCSB PDB - 3VN2: Crystal structure of PPARgamma complexed with telmisartan [Internet]. United States: RCSB PDB. 2012 [cited 2025 Jul 4]. Available from: https://www.rcsb.org/structure/3VN2.
[2] Zhang H, Unal H, Desnoyer R, Han GW, Patel N, Katritch V, *et al.* RCSB PDB - 4ZUD: Crystal structure of human angiotensin receptor in complex with inverse agonist olmesartan at 2.8Å resolution. [Internet]. United States: RCSB PDB. 2015 [cited 2025 Jul 4]. Available from: https://www.rcsb.org/structure/4ZUD.

olmesartan with ATR were loaded into SYBYL-X® v1.1 (Ash *et al.*, 2010). All unnecessary moieties including the bound small molecule, telmisartan and olmesartan respectively, repeating sub-units, non-critical water molecules were removed to create the respective apo-proteins (Ellul & Shoemake, 2017).

2.4.7 Identification of Lipinski Rule Compliant Hits

Hit molecules identified from ZINCPharmer® (Koes & Camacho, 2012) underwent a second filtration through MONA® (Hilbig & Rarey, 2015) by applying filters according to Lipinski's Rules (Lipinski *et al.*, 2012). The initial filtration carried out in ZINCPharmer® did not allow for consideration of the number of HBAs and HBDs of the hit molecules. This limitation was addressed through this second filtration where the filters applied in MONA® were 1-10 HBAs and Lipinski acceptors, 1-5 HBDs and Lipinski donors, maximum calculated Log P (cLogP) of 5, and a MW between 1Da and 500Da. This ensured that any potential Lipinski Rule violators (with respect to HBAs and HBDs) would be excluded. The filtered set of molecules in *.mol2* format to be read into SYBYL-X® v1.1 (Ash *et al.*, 2010).

2.4.8 Uploading Hits into Protomols

The filtered set of molecules were read into the modelled protomols in SYBYL-X®. The binding affinity of hits for both protomols were calculated by uploading the filtered set of molecules into SYBYL-X® v1.1 (Ash *et al.*, 2010) and docking them separately into the protomols for both the PPARγ and ATR. The molecules were ranked separately in order of binding affinity to both protomols in SYBYL-X® v1.1 (Ash *et al.*, 2010) where binding affinity is expressed as a total score. Highest ranking Lipinski rule compliant hits

were identified. These molecules were further screened for toxicity using ProTox 3.0® *(*Banerjee *et al.,* 2024*)* where the predicted oral toxicity of the ZINC molecules was predicted by inputting the Simplified Molecular Input Line Entry System (SMILES) formula of the molecules into the ProTox 3.0® virtual laboratory. ZINC molecules were also screened specifically for cardiotoxicity as an organ-specific effect and for carcinogenicity as a specific toxicity end point (Banerjee *et al.*, 2024). These specific effects were selected on the basis of reports published by the Medicines and Healthcare products Regulatory Agency (MHRA) on the safety of the pioglitazone, a benzimidazole thiazolidinedione, used in the treatment of T2DM. Pioglitazone has been associated with a risk of cardiac failure when used in combination with insulin[3] and a small increased risk of bladder cancer.[4]

[3] Medicines and Healthcare products Regulatory Agency. Insulin combined with pioglitazone: risk of cardiac failure [Internet]. United Kingdom: GOV.UK. 2014 [cited 2025 Jul 26]. Available from: https://www.gov.uk/drug-safety-update/insulin-combined-with-pioglitazone-risk-of-cardiac-failure.

[4] Medicines and Healthcare products Regulatory Agency. Pioglitazone: risk of bladder cancer [Internet]. United Kingdom: GOV.UK. 2014 [cited 2025 Jul 26]. Available from: https://www.gov.uk/drug-safety-update/pioglitazone-risk-of-bladder-cancer.

2.5 *de Novo* Design

In this phase of the study, a SBDD approach was adopted were fragments modelled from the lead molecule, termed as seed structures, were docked into the receptor LBPs and allowed to grow at predesignated researcher-defined *loci*.

2.5.1 Optimal Conformer Identification

PDB crystallographic depositions 3VN2[1] and 4ZUD[2] were read separately into SYBYL-X® v1.1 (Ash *et al.*, 2010). The *apo* receptor proteins (PPARγ and ATR respectively) were exported in *.pdb* format by removing the bound small molecules and unnecessary moieties including any repeating sub-units and non-critical water molecules. The small molecules, telmisartan and olmesartan, previously bound to their respective receptors as obtained from the RCSB PDB were also exported separately and unbound in their ideal conformation as *.mol2* files. Using the 'Similarity Suite' function on SYBYL-X® v1.1 (Ash *et al.*, 2010), telmisartan and olmesartan *.mol2* files were read in separately as template molecules while HTR-04, the lead molecule of the study (Chittiboyina *et al.*, 2009) was read in as a ligand source, also in *.mol2* format. From the 'Surflex-Sim' feature, 'Consider Ring Flexibility' was selected to allow the ligand source ring structures to rotate. This process aligned the lead molecule in similar spatial arrangements as telmisartan and olmesartan within their respective receptors. This process was carried out to accommodate the lead molecule into the receptor LBPs and identify the ideal conformation for docking. The ideal conformations are identifiable as file names

[1] Amano Y. RCSB PDB - 3VN2: Crystal structure of PPARgamma complexed with telmisartan [Internet]. United States: RCSB PDB. 2012 [cited 2025 Jul 4]. Available from: https://www.rcsb.org/structure/3VN2.
[2] Zhang H, Unal H, Desnoyer R, Han GW, Patel N, Katritch V, *et al.* RCSB PDB - 4ZUD: Crystal structure of human angiotensin receptor in complex with inverse agonist olmesartan at 2.8Å resolution. [Internet]. United States: RCSB PDB. 2015 [cited 2025 Jul 4]. Available from: https://www.rcsb.org/structure/4ZUD.

corresponding to ideal conformation in denoted by a '*J*'. These were exported and saved as *.mol2* files. This process was carried out as the lead molecule was identified from the literature review carried out and is not available bound to the target receptors in the RCSB PDB. These conformations are depicted in Figures 3.19 and 3.20.

2.5.2 2D Topology Map Generation

In the *de novo* design approach, 2D topology maps describing the critical interactions between HTR-04 (Chittiboyina *et al.*, 2009) and the LBPs of PPARγ and ATR respectively were generated using BIOVIA Discovery Studio Visualizer® v24.1 (Baroroh *et al.*, 2023). This was carried out by uploading the *apo* PPARγ and ATR receptors respectively in *.pdb* format into BIOVIA Discovery Studio® v24.1(Baroroh *et al.*, 2023) together with the HTR-04 lead molecule (Chittiboyina *et al.*, 2009) in *.mol2* format. The 2D topology maps generated are depicted in Figures 3.21 and 3.22.

2.5.3 Modelling of Seed Structures

The interactions described in the 2D topology maps guided the modelling of seed structures from the optimal HTR-04 (Chittiboyina *et al.*, 2009) conformers within each *apo* receptor in SYBYL-X® v1.1 (Ash *et al.*, 2010). Areas of unfavourable interactions (illustrated in red in the 2D topology maps above) between the hybrid benzimidazole molecule HTR-04 (Chittiboyina *et al.*, 2009) and the amino acids within the LBP of the PPARγ and ATR were preferentially removed during the seed structure modelling process while the benzimidazole scaffold was maintained in most seed structures.

Seed structures were modelled in SYBYL-X® v1.1 (Ash *et al.*, 2010) where the files containing the optimal conformations of HTR-04 (Chittiboyina *et al.*, 2009) within the

PPARγ and ATR LBPs were imported individually in *.mol2* format. Atoms were individually selected and removed by selecting 'Edit', followed by 'Delete', followed by 'Selected Atoms'. Atoms designated for potential molecular growth were determined by selecting the desired atom, selecting 'Edit', then 'Atom', followed by 'Modify Atom Type' and finally selecting 'H.spc' (special hydrogen atom). When selecting the type of bond desired in the 'Select Bond Type' tab, a single bond was opted for as this allows for more freedom during molecular growth, unlike multiple bonds which confer rigidity. Seed structures were exported individually, named sequentially in numerical order and saved in *.mol2* format. A total 30 seed structures were modelled in SYBYL-X® v1.1 (Ash *et al.*, 2010) based on the two confromations of HTR-04 (Chittiboyina *et al.*, 2009) i.e., 15 seed structures for each conformation.

2.5.4 Ligand Binding Affinity Calculation

Ligand binding affinity (LBA) (measured as a dissociation constant [pKd]) of the molecules bound to the target receptors PPARγ and ATR as obtained from their respective PDB crystallographic depositions was measured in this step. This was conducted to establish a baseline affinity for comparison with molecules to be designed *de novo*, which must exhibit a greater affinity to the target receptors than the bound molecules. This process was carried out in X-SCORE® v1.3 (Wang *et al.*, 2002) where the *apo* PPARγ and ATR were read in as *.pdb* files and the bound molecules, telmisartan and olmesartan respectively, were read in as a *.mol2* files.

2.5.5 Modelling of LBPs

3D models of receptor LBPs were created in LigBuilder® v1.2 (Yuan *et al.*, 2020) using the 'Pocket' module, delineating the area in which seeds may be docked and detailing the steric and electrostatic interactions that may be formed between the docked seed and the receptor LBP during molecular growth (Yuan *et al.*, 2020). The *apo* PPARγ and ATR proteins were inputted into LigBuilder® v1.2 in *.pdb* format as the receptor files while the optimal HTR-04 (Chittiboyina *et al.*, 2009) conformations were stored in *.mol2* format as the ligand file using the *pocket.index* text file. Using the Ubuntu® terminal, commands were given to generate the LBP 3D model for the PPARγ. The process was repeated for the generation of the ATR LBP 3D model. For each receptor, a '*key_site_file*' and '*pharmacophore_file*' were generated. The '*key_site_file*' contains the critical interaction sites within the LBP while the '*pharmacophore_file*' identifies pharmacophoric structures and atom types that the docked molecule must possess at specified loci in order for it to forge a favourable interaction with the receptor LBP (Wang *et al.*, 2000). A '*pocket.text*' and '*grid.text*' file were also generated to be used in the following step of seed structure growth.

2.5.6 Seed Structure Growth

The 'Grow' and 'Link' modules of LigBuilder® v1.2 (Yuan *et al.*, 2020) were utilised to determine which seeds sustain molecular growth at predesignated loci defined by special hydrogen atoms (H.spc). The 'Grow' module allows for unilateral growth from the predesignated special hydrogen atom. The 'Link' module allows for bilateral growth from two predesignated special hydrogen atoms, whereby such growth allows for the two fragments of the same seed structure to link into one whole molecule. Molecular growth, both through the 'Grow' and 'Link' modules is carried out rationally by LigBuilder® v1.2

by virtue of the availability of 3D models of receptor LBPs and the amino acids that lie within these LBPs. LigBuilder® v1.2 utilises these 3D LBP models to conduct molecular growth with structures of high affinity to LBPs (Yuan *et al.*, 2020) . Of the 15 seed structures modelled in SYBYL-X® v1.1 (Ash *et al.*, 2010) for each of the two conformations of HTR-04 (Chittiboyina *et al.*, 2009), 10 were designed for the 'Grow' module and 5 were designed for the 'Link' module. The seed structures designed were read in as the seed ligand files in *.mol2* format into the respective '*grow.index*' or '*link.index*' text files within the respective 'Grow' and 'Link' modules, depending on whether seed structures were designed for growth or for linkage. The '*pocket.text*' and '*grid.text*' files generated in the preceding step were also inputted in this step. The text file also contains the molecular databases '*fragment.mdb*' containing fragments used for seed growth, '*forbidden.mdb*' consisting of fragments which are excluded as they are not synthesisable, and '*toxicity.mdb*' composed of fragments which are excluded as they are known to be toxic. Using the Ubuntu® terminal, commands were given depending on whether the 'Grow' or 'Link' module was in use.

These commands ran the software to attempt molecular growth. One seed structure sustained molecular growth using the 'Grow' module and is depicted in Figure 3.29. The atom circled in red denotes the locus of the special hydrogen atom and is the atom at which molecular growth occurred. No seed structures sustained molecular growth using the 'Link' module. The parameters set within the 'Grow' and 'Link' modules for seed growth were set as shown in Table 2.2.

Table 2.2: Parameters set within the 'Grow' and 'Link' modules in LigBuilder® v1.2 (Yuan *et al.*, 2020) for seed growth.

Parameter	'Grow' Module	'Link' Module
Maximal MW (Da)	600	600
Minimal MW (Da)	300	300
Maximal LogP	6.00	6.00
Minimal LogP	3.00	3.00
Maximal HBDs	6	6
Minimal HBDs	2	2
Maximal HBAs	6	6
Minimal HBAs	2	2
Maximal pKd	10.00	10.00
Minimal pKd	5.00	5.00

2.5.7 Identification of Lipinski Rule Compliant Structures

After successful molecular growth, the 'Process' module of LigBuilder® v1.2 (Yuan *et al.*, 2020) was used to generate a molecular database containing the molecules obtained from the seed structure that sustained molecular growth, as per the set parameters as shown in Table 2.3. The '*process.index*' file is used to filter the 200 highest-affinity molecules and export them into a molecular database. The database details the physicochemical properties of each molecule generated including MW, partition coefficient expressed as CLogP, binding score (expressed as pKd) and chemical score. The molecular database was extracted into Microsoft Excel® where filters were applied to ensure Lipinski Rule compliance (Lipinski *et al.*, 2012) and a LBA greater than that of

the molecules bound to the target receptors PPARγ and ATR as obtained from their respective PDB crystallographic depositions. The filters applied were a maximum MW of 500 Da, a maximum cLogP of 5 and a minimum binding score (pKd) of 7.08, greater than LBA of olmesartan to the ATR as found in PDB crystallographic depositions 4ZUD[2]. The HBDs and HBAs of the Lipinski Rule compliant molecules with a binding score (pKd) greater than 7.08 was found using LigBuilder® v1.2 (Yuan *et al.*, 2020) by importing the molecules into LigBuilder® v1.2 as *.mol2* files. Molecules with more than 10 HBAs or more than 5HBDs (Lipinski *et al.*, 2012) were considered to be Lipinski Rule violators and were excluded. The molecules that met the inclusion criteria were further screened for toxicity using ProTox 3.0® (Banerjee *et al.*, 2024) by inputting the SMILES formula of the molecule into the ProTox 3.0® virtual laboratory (Banerjee *et al.*, 2024).

Table 2.3: Parameters set within the 'Process' module in LigBuilder® v1.2 (Yuan *et al.*, 2020).

Parameter	**'Process' Module**
Maximal MW (Da)	600
Minimal MW (Da)	300
Maximal LogP	6.00
Minimal LogP	3.00
Maximal pKd	10.00
Minimal pKd	5.00

[2] Zhang H, Unal H, Desnoyer R, Han GW, Patel N, Katritch V, *et al.* RCSB PDB - 4ZUD: Crystal structure of human angiotensin receptor in complex with inverse agonist olmesartan at 2.8Å resolution. [Internet]. United States: RCSB PDB. 2015 [cited 2025 Jul 4]. Available from: https://www.rcsb.org/structure/4ZUD.

2.5.8 Calculating Binding Score for PPARγ

Since the seed structure that generated molecules *de novo* was based on the ligand-protein interactions between HTR-04 (Chittiboyina *et al.*, 2009) and ATR, the resulting binding scores of the generated molecules reflect the LBA for the ATR. Binding scores for PPARγ were evaluated independently. Using the 'Similarity Suite' function on SYBYL-X® v1.1 (Ash *et al.*, 2010) unbound telmisartan was read in as a template molecule in *.mol2* format while the 10 highest affinity molecules derived from *de novo* seed fragment growth were read in separately as ligand sources, also in *.mol2* format. From the 'Surflex-Sim' feature, 'Consider Ring Flexibility' was selected to allow the ligand source ring structures to rotate. This process aligned the molecules designed *de novo* in similar spatial arrangements as that occupied by telmisartan within their PPARγ receptor. This process was carried out to accommodate the molecules into the receptor LBP and identify the ideal conformation for docking. The ideal conformations are identifiable as file names corresponding to ideal conformation in denoted by a '*J*'. These conformations were exported and saved as *.mol2* files.

LBA (pKd) of the *de novo* molecules to the PPARγ as obtained from PDB crystallographic depositions 3VN2[1] was measured in X-SCORE® v1.3 (Wang *et al.*, 2002) where the *apo* PPARγ was read in *.pdb* format and the molecules were read in individually in *.mol2* format.

[1] Amano Y. RCSB PDB - 3VN2: Crystal structure of PPARgamma complexed with telmisartan [Internet]. United States: RCSB PDB. 2012 [cited 2025 Jul 4]. Available from: https://www.rcsb.org/structure/3VN2.

Chapter 3

Results

3.1 Virtual Screening Results

3.1.1 Generation of a Consensus Pharmacophore

The generation of a consensus pharmacophore involved the rendering of the individual pharmacophores of unbound telmisartan (Figure 3.3); unbound olmesartan (Figure 3.8); and the hybrid benzimidazole HTR-04 (Figure 3.12) (Chittiboyina *et al.*, 2009). The consensus pharmacophore consists of a 3D arrangement of molecular features, essential for the biological activity of a ligand and the interaction of the ligand with a receptor. Table 3.1 illustrates the pharmacophoric features and their significance as depicted in LigandScout® v4.4 (Wolber & Langer, 2005).

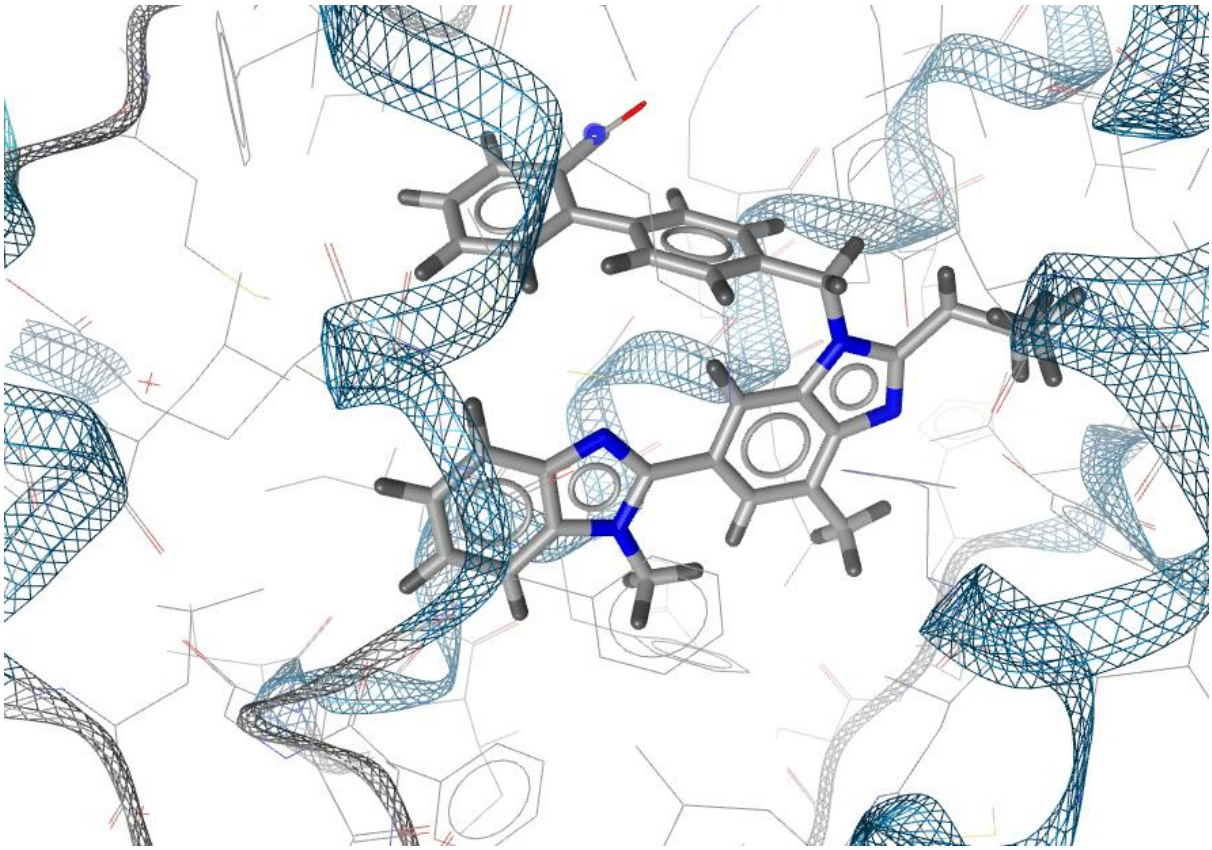

Figure 3.1: Bioactive conformation of telmisartan bound to PPARγ as rendered in LigandScout® v4.4 (Wolber & Langer, 2005).

Analysis of the PPARγ-telmisartan complex (as described in PDB 3VN2[1]) in LigandScout® v4.4 (Wolber & Langer, 2005) revealed the key interactions between telmisartan and the amino acid residues within the PPARγ LBP. A pharmacophore was generated (Figure 3.3) and superimposed onto the bioactive conformation of unbound telmisartan (Figure 3.4). A 2D interaction map illustrating the critical residue contacts was rendered (Figure 3.5).

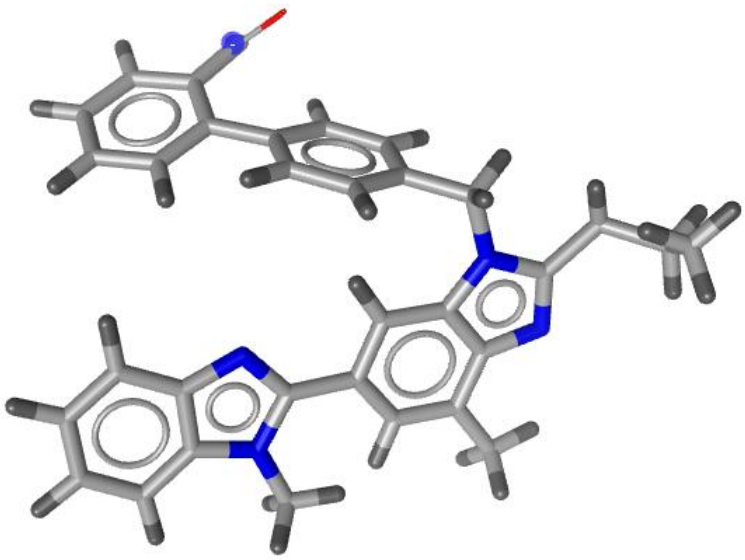

Figure 3.2: Bioactive conformation of unbound telmisartan as rendered in LigandScout® v4.4 (Wolber & Langer, 2005).

[1] Amano Y. RCSB PDB - 3VN2: Crystal structure of PPARgamma complexed with telmisartan [Internet]. United States: RCSB PDB. 2012 [cited 2025 Jul 4]. Available from: https://www.rcsb.org/structure/3VN2.

Table 3.1: Table of pharmacophoric features as depicted in LigandScout® v4.4.

Reproduced from: Wolber G, Langer T. LigandScout: 3-D Pharmacophores Derived from Protein-Bound Ligands and their Use as Virtual Screening Filters. Journal of Computer-Aided Molecular Design. 2005; 45 (1): 160-169. doi: 10.1021/ci049885e.

Depiction in LigandScout®	**Pharmacophore Feature**	**Abbreviation**
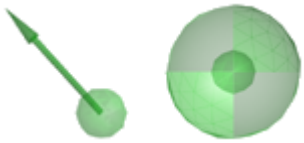	Hydrogen Bond Donor	HBD
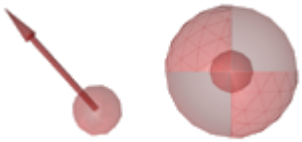	Hydrogen Bond Acceptor	HBA
	Negative Ionizable Area	NI
	Hydrophobic Interactions	HI
	Aromatic Ring	AR
	Halogen Bond Donor	XBD

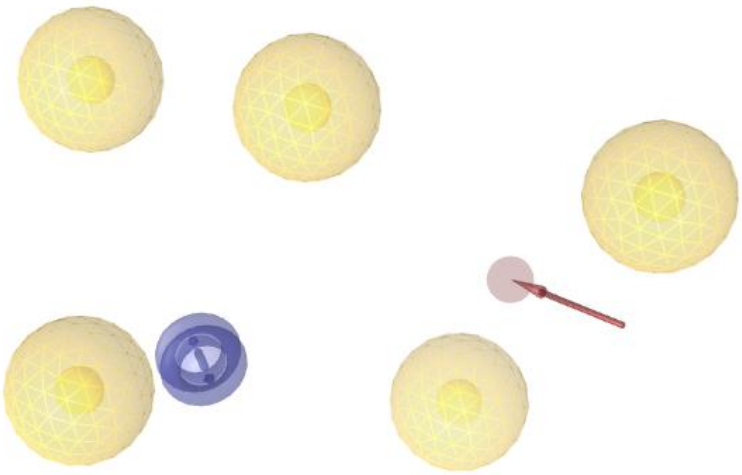

Figure 3.3: Pharmacophoric structure of telmisartan describing the critical contacts of the molecule with the LBP of the PPARγ as rendered in LigandScout® v4.4 (Wolber & Langer, 2005).

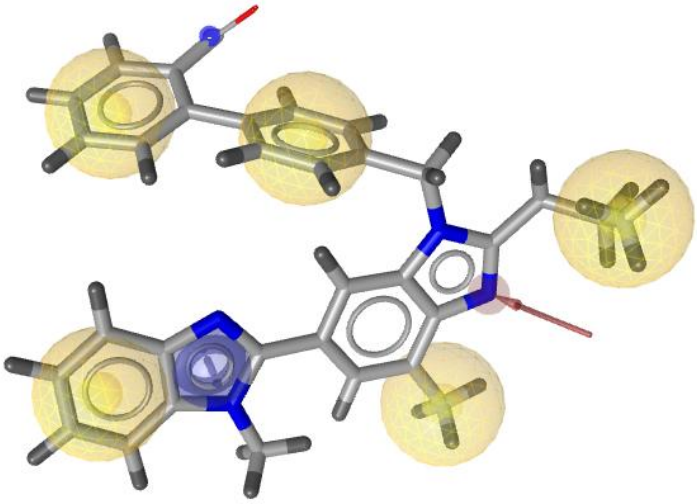

Figure 3.4: Bioactive conformation of telmisartan superimposed onto its pharmacophore as rendered in LigandScout® v4.4 (Wolber & Langer, 2005).

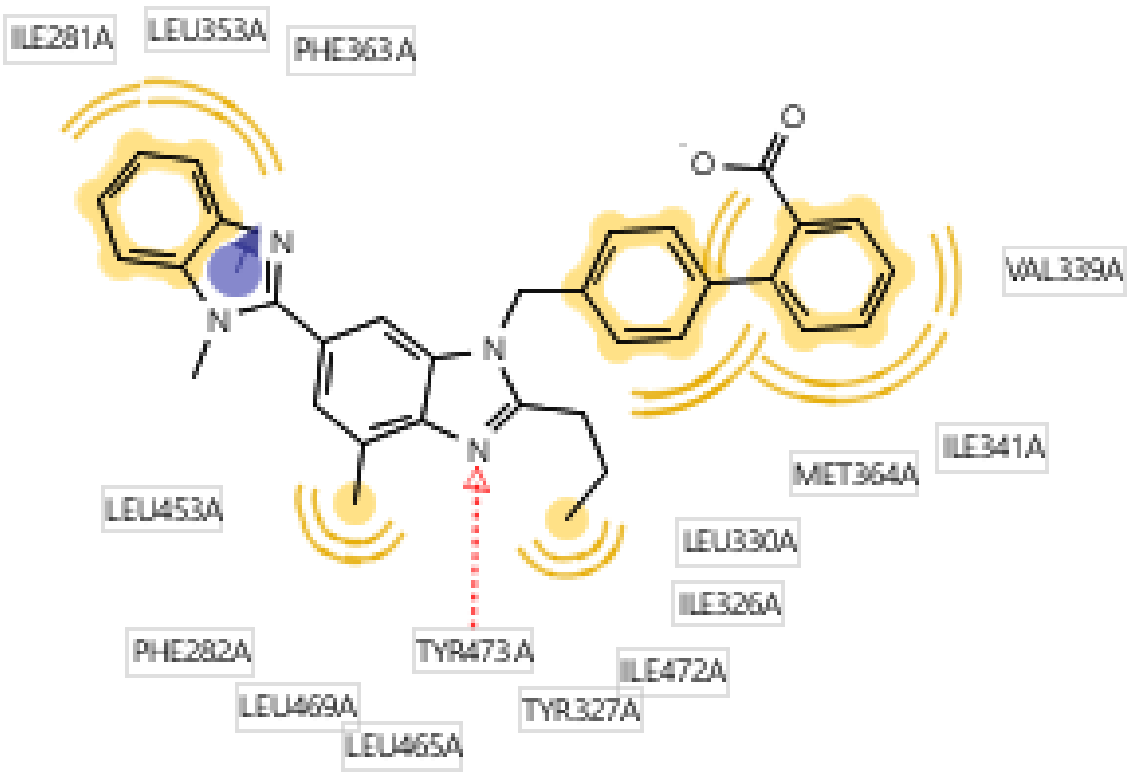

Figure 3.5: 2D bioactive conformation of telmisartan describing the critical contacts of the telmisartan molecule with the amino acids at the LBP of PPARγ as rendered in LigandScout® v4.4 (Wolber & Langer, 2005).

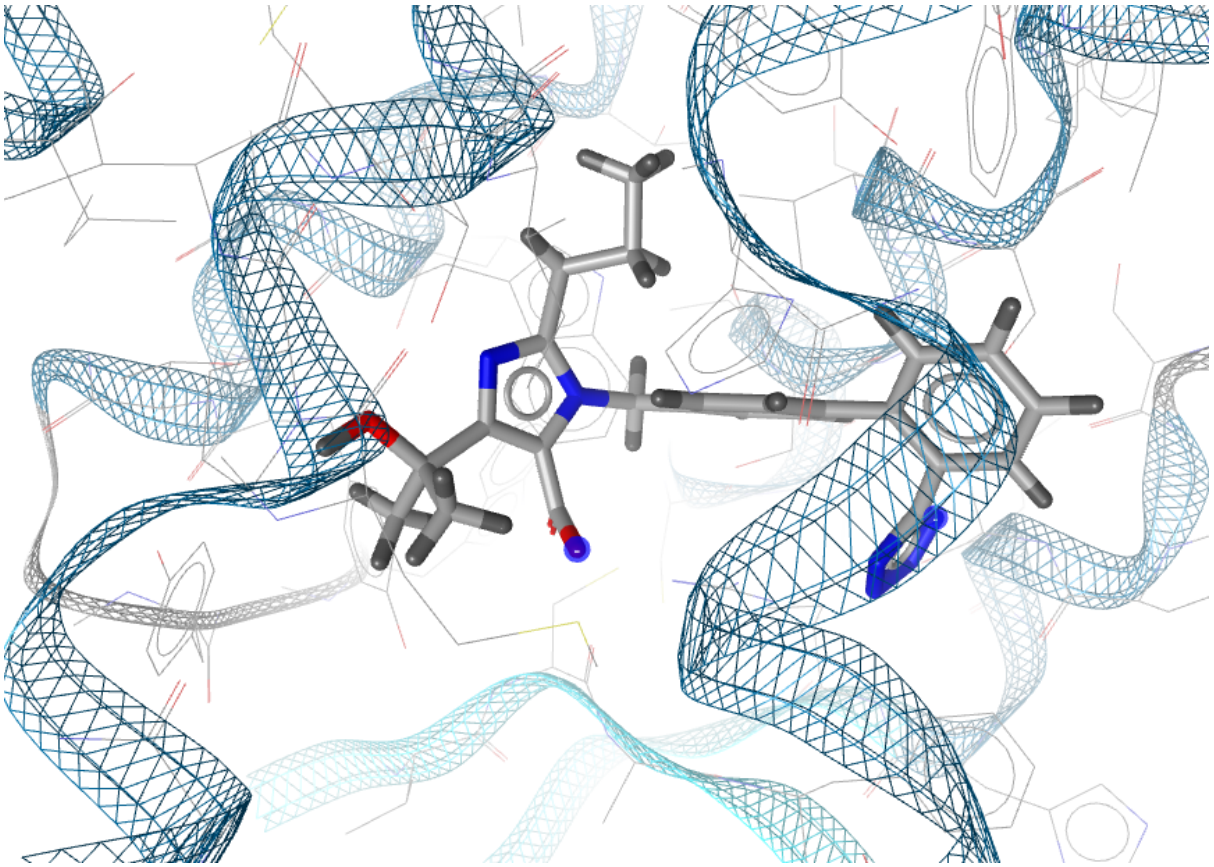

Figure 3.6: Bioactive conformation of olmesartan bound to the ATR as rendered in LigandScout® v4.4 (Wolber & Langer, 2005).

Analysis of the ATR–olmesartan complex as described in PDB crystallographic deposition 4ZUD[2] in LigandScout® v4.4 identified the key interactions of olmesartan and the amino acid residues within the ATR LBP. A pharmacophore model was generated (Figure 3.7) and superimposed with the bioactive conformation of unbound olmesartan (Figures 3.8 and 3.9). A 2D interaction map, also generated in LigandScout® v4.4 (Wolber & Langer, 2005) further illustrated the critical residue contacts (Figure 3.10).

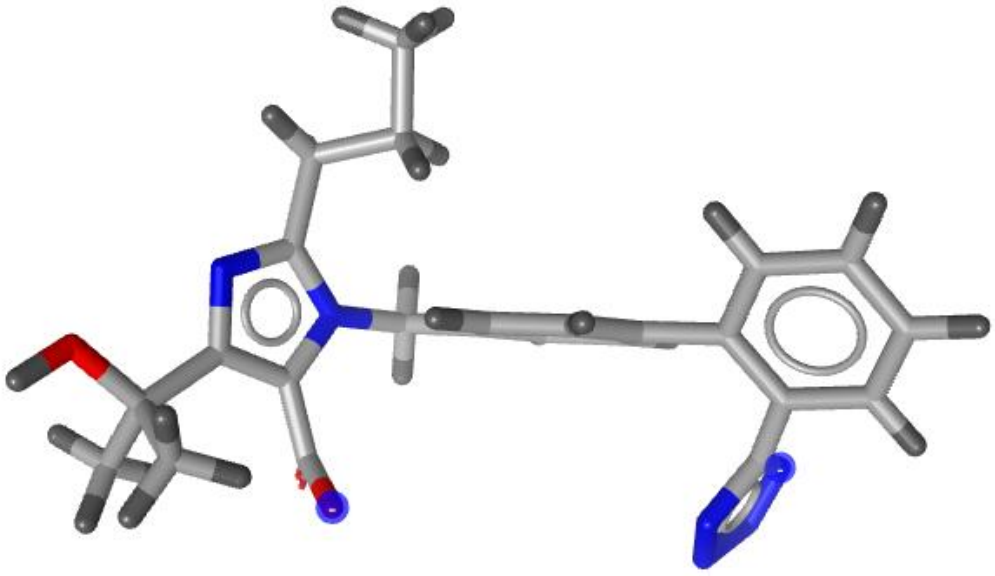

Figure 3.7: Bioactive conformation of unbound olmesartan as rendered in LigandScout® v4.4 (Wolber & Langer, 2005).

[2] Zhang H, Unal H, Desnoyer R, Han GW, Patel N, Katritch V, *et al.* RCSB PDB - 4ZUD: Crystal structure of human angiotensin receptor in complex with inverse agonist olmesartan at 2.8Å resolution. [Internet]. United States: RCSB PDB. 2015 [cited 2025 Jul 4]. Available from: https://www.rcsb.org/structure/4ZUD.

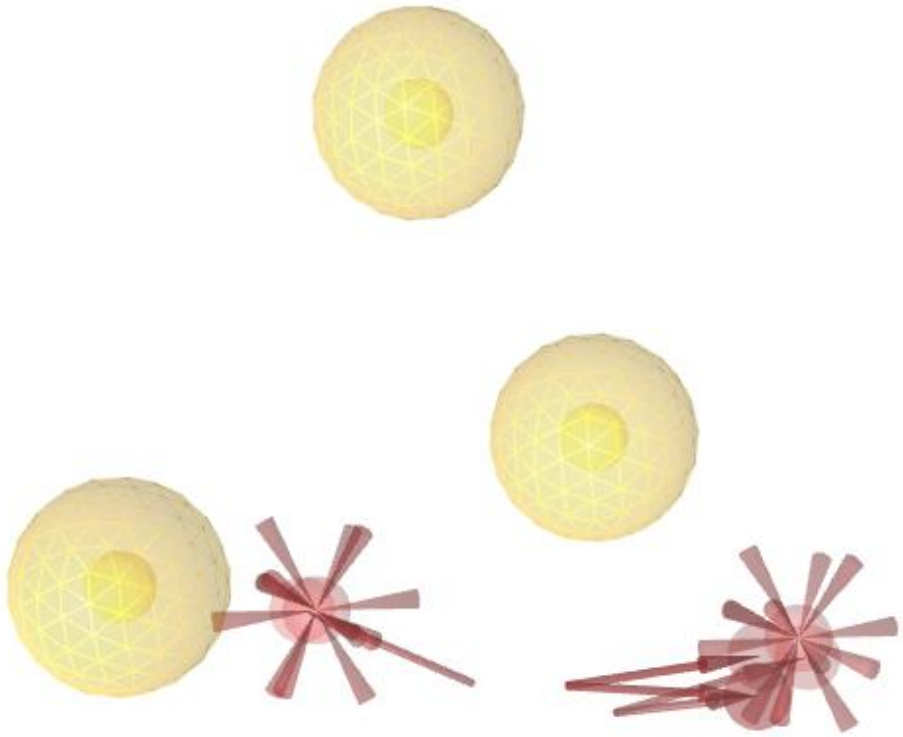

Figure 3.8: Pharmacophoric structure of olmesartan describing the critical contacts of the molecule with the LBP of the ATR receptor as rendered in LigandScout® v4.4 (Wolber & Langer, 2005).

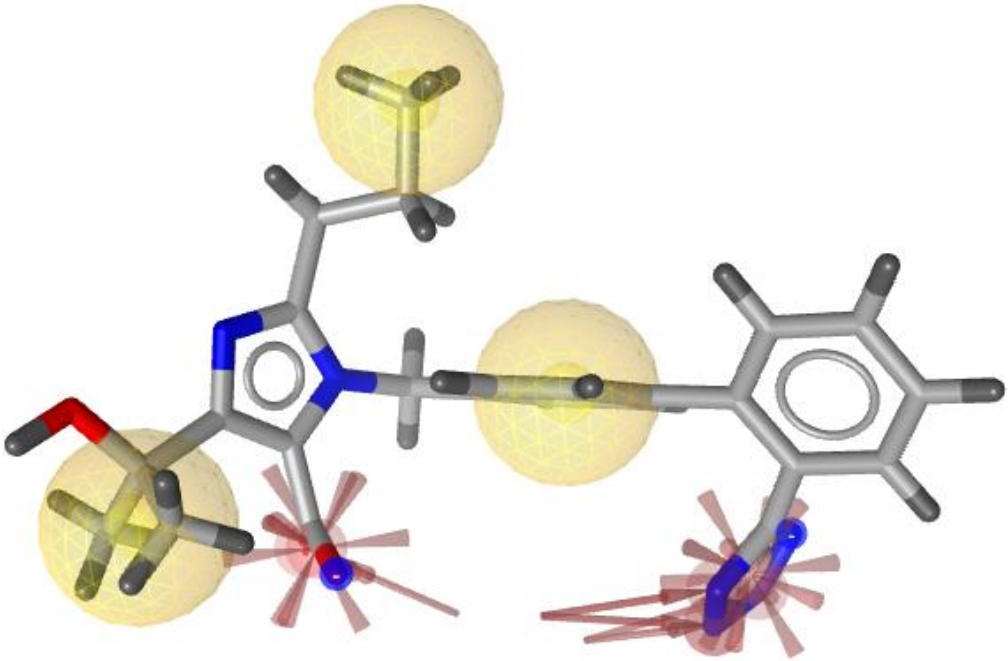

Figure 3.9: Bioactive conformation of olmesartan superimposed onto its pharmacophore as rendered in LigandScout® v4.4 (Wolber & Langer, 2005).

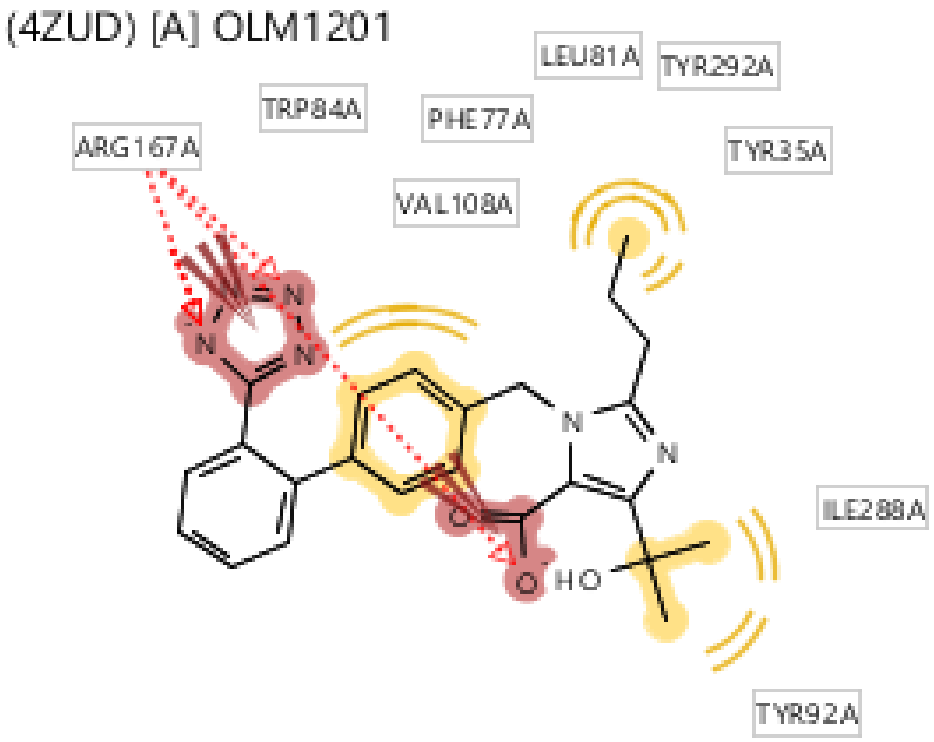

Figure 3.10: 2D bioactive conformation of olmesartan describing the critical contacts of the molecule with the LBP of ATR as rendered in LigandScout® v4.4 (Wolber & Langer, 2005).

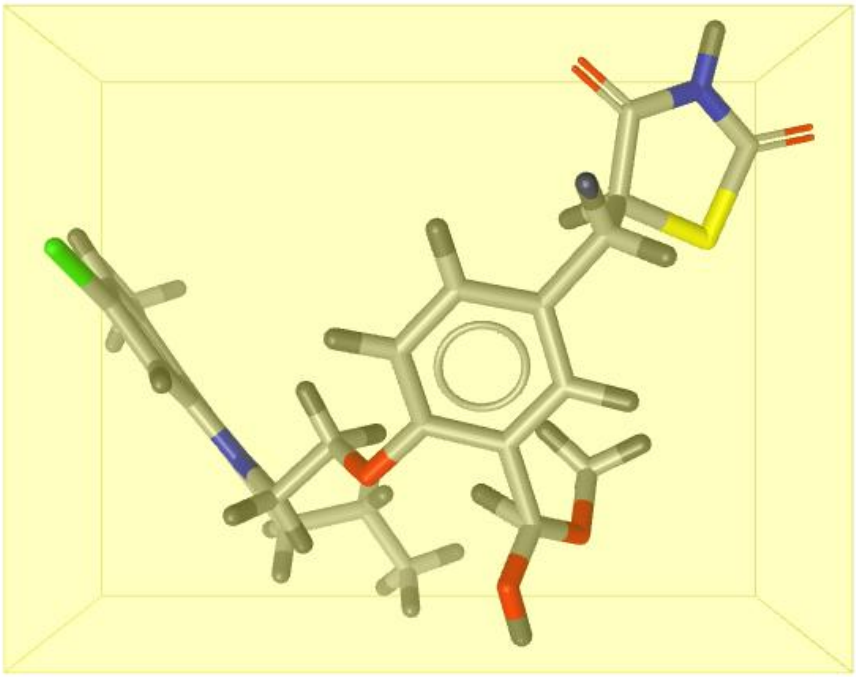

Figure 3.11: Structure of unbound hybrid benzimidazole HTR-04 (Chittiboyina *et al.*, 2009) as drawn in SYBYL-X® v1.1 (Ash *et al.*, 2010) and rendered in LigandScout® v4.4 (Wolber & Langer, 2005).

Analysis of the hybrid benzimidazole HTR-04 (Chittiboyina *et al.*, 2009) in LigandScout® v4.4 (Wolber & Langer, 2005) revealed its key interactions with amino acid residues in the PPARγ LBP. A pharmacophore model was generated (Figure 3.12) and superimposed with the unbound conformation of HTR-04 (Figure 3.13).

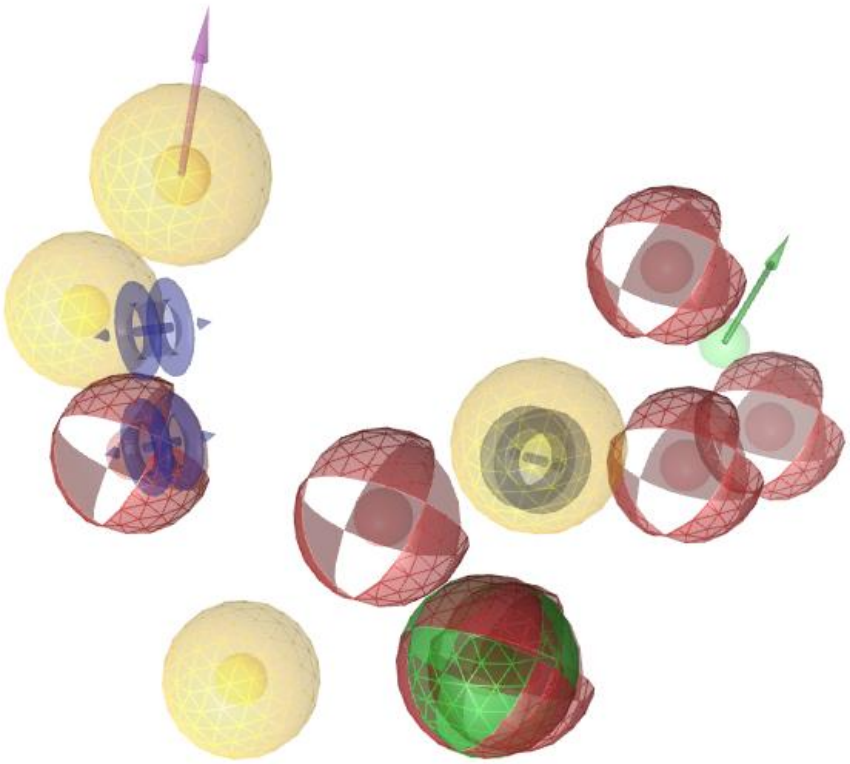

Figure 3.12: Pharmacophoric structure of hybrid benzimidazole HTR-04 (Chittiboyina *et al.*, 2009) describing the critical contacts of the molecule with the LBP of the PPARγ as rendered in LigandScout® v4.4 (Wolber & Langer, 2005).

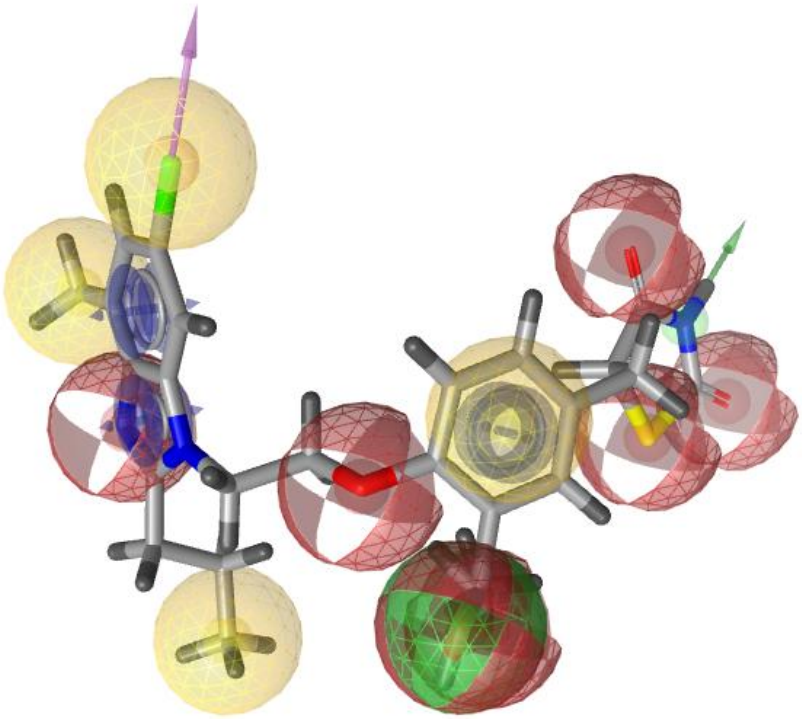

Figure 3.13: Hybrid benzimidazole HTR-04 (Chittiboyina *et al.*, 2009) superimposed onto its pharmacophore as rendered in LigandScout® v4.4 (Wolber & Langer, 2005).

The process of superimposing the individual pharmacophores derived from all three molecules, telmisartan, olmesartan, and HTR-04 (Chittiboyina *et al.*, 2009), made it possible to identify the overlapping features and key interaction points that are shared between the compounds, expressed as a consensus pharmacophore in Figure 3.14. This comparative alignment revealed the structural elements common to all three molecules along with the critical functional groups that contribute to receptor binding. The resulting consensus pharmacophore provides a unified model consisting of the critical spatial orientation and electronic properties necessary for stable interactions with the PPARγ and ATR. This model serves as a valuable framework for understanding the molecular basis

of ligand recognition and can guide the design of future molecules with improved potency and specificity.

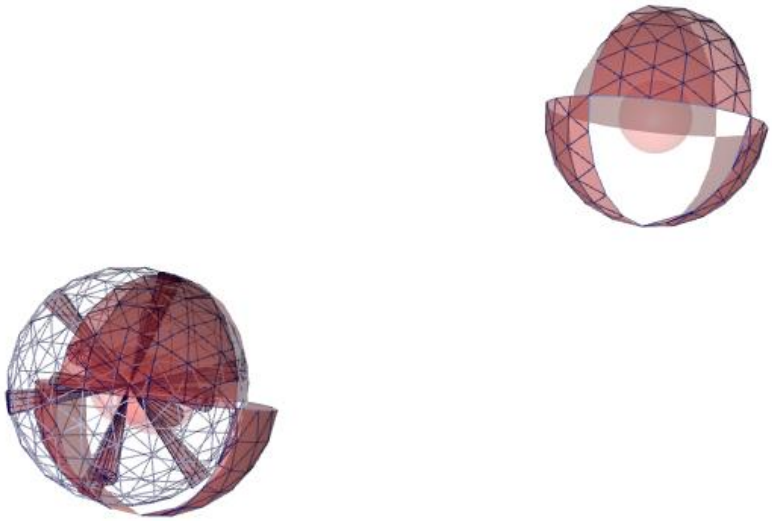

Figure 3.14: Shared-feature pharmacophoric structure of hybrid benzimidazole HTR-04 (Chittiboyina *et al.*, 2009), telmisartan, and olmesartan as rendered in LigandScout® v4.4 (Wolber & Langer, 2005).

3.1.2 Analysis of Hit Molecules

From the ZINCPharmer® query search, a total of 1468 hits were identified, of which 300 hits were obtained from ZINC Purchasable, 258 hits from ZINC Purchasable Thiols, 23 hits from ZINC Drug Database, 148 hits from ZINC in Man, 140 hits from ZINC Drug Database (Metabolites), 299 hits from ZINC Natural Derivatives, and 300 hits from ZINC Natural Products (Koes & Camacho, 2012). After removing duplicate molecules and applying a second filtration through MONA®, 519 Lipinski Rule compliant hit molecules

were identified. These 519 molecules were docked into the generated protomols of both the PPARγ and ATR, depicted in Figures 3.15 and 3.16, respectively.

ZINC00188045 was identified as the lead-like molecule with the highest affinity for the PPARγ protomol with a total score of 5.58. Similarly, ZINC48322609 was identified as the lead-like molecule with the highest affinity for the ATR protomol with a total score of 5.08. The 10 lead-like molecules with the highest combined affinity for both the PPARγ and the ATR protomol were identified and their 2D structures are depicted in Table 3.2. The physicochemical properties of the highest-affinity lead-like molecules are tabulated in Table 3.3.

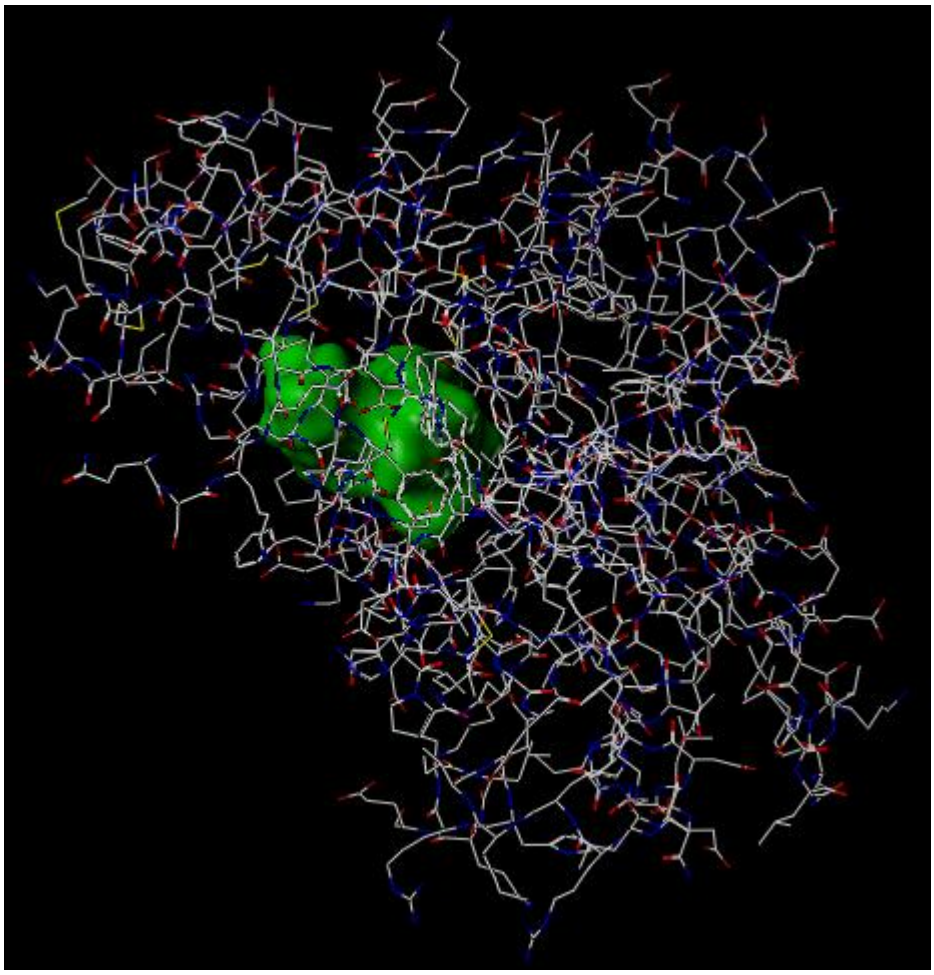

Figure 3.15: Protomol describing the energetically unsatisfied space within the PPARγ as described in PDB crystallographic deposition 3VN2[1], rendered in SYBYL-X® v1.1 (Ash *et al.*, 2010).

[1] Amano Y. RCSB PDB - 3VN2: Crystal structure of PPARgamma complexed with telmisartan [Internet]. United States: RCSB PDB. 2012 [cited 2025 Jul 4]. Available from: https://www.rcsb.org/structure/3VN2.

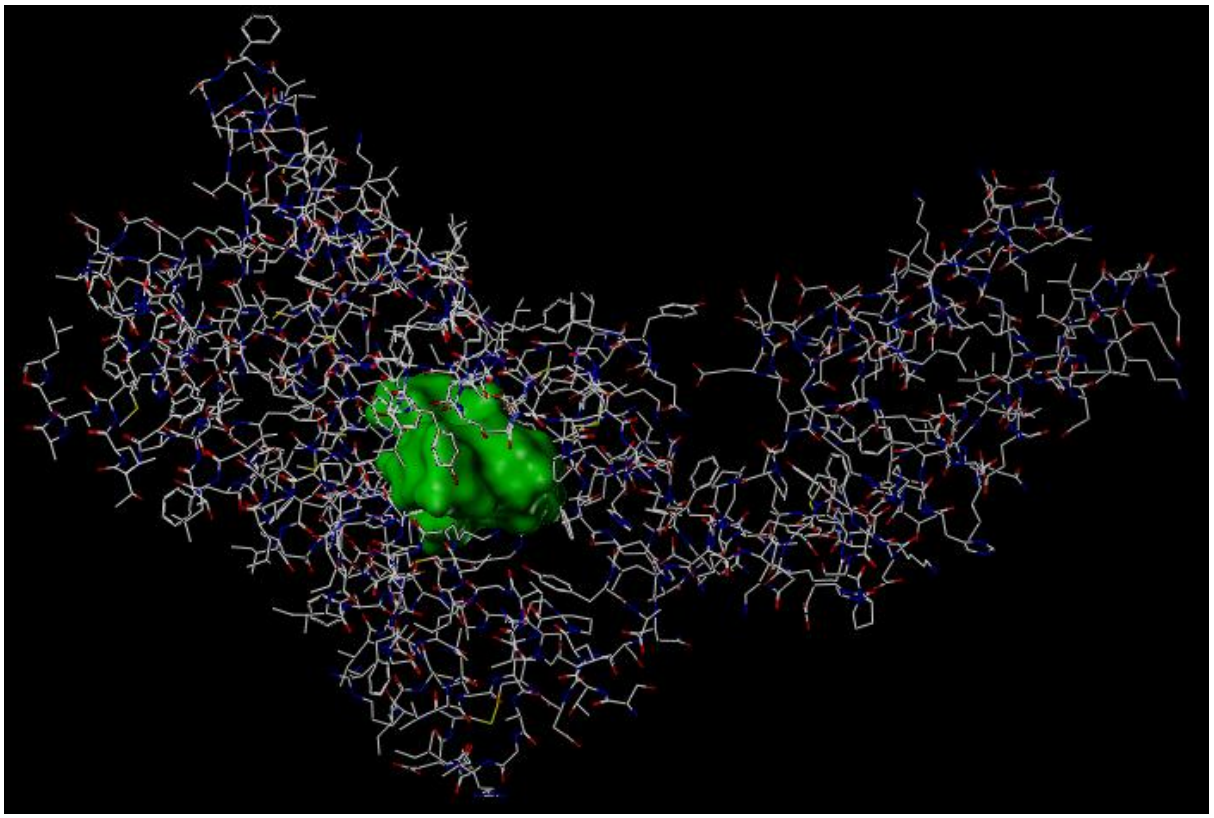

Figure 3.16: Protomol describing the energetically unsatisfied space within the ATR as described in PDB crystallographic deposition 4ZUD[2], rendered in SYBYL-X® v1.1 (Ash *et al.*, 2010)

[2] Zhang H, Unal H, Desnoyer R, Han GW, Patel N, Katritch V, *et al.* RCSB PDB - 4ZUD: Crystal structure of human angiotensin receptor in complex with inverse agonist olmesartan at 2.8Å resolution. [Internet]. United States: RCSB PDB. 2015 [cited 2025 Jul 4]. Available from: https://www.rcsb.org/structure/4ZUD.

Table 3.2: Table depicting 2D molecular structure of the highest affinity Lipinski Rule compliant molecules (n=10).

ZINC Code	2D Structures
ZINC48322609	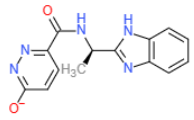
ZINC92968473	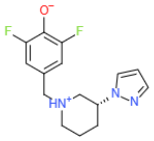
ZINC00188045	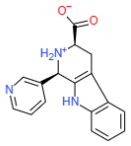
ZINC94889747	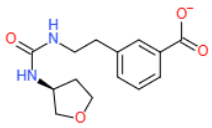
ZINC92203809	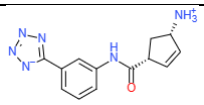
ZINC19703382	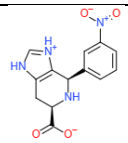
ZINC56650139	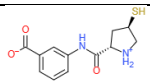
ZINC00188053	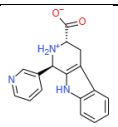
ZINC03985304	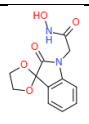
ZINC12546012	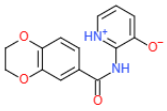

Table 3.3: Physicochemical properties of the highest affinity Lipinski Rule compliant molecules (n=10).

ZINC Code	PPARγ Affinity (Total Score)	ATR Affinity (Total Score)	cLogP	HBDs	HBAs	Rotatable Bonds	MW (Da)
ZINC48322609	4.85	5.08	2.38	2	5	4	282.283
ZINC92968473	5.04	4.61	3.29	1	1	3	293.317
ZINC00188045	5.58	3.66	1.46	2	2	2	293.326
ZINC94889747	4.81	4.42	0.46	2	5	7	277.3
ZINC92203809	5.32	3.79	-0.31	2	5	4	270.296
ZINC19703382	5.33	3.75	-0.06	3	3	3	288.263
ZINC56650139	4.49	4.49	0.26	3	4	3	266.322
ZINC00188053	4.13	4.77	1.46	2	2	2	293.326
ZINC03985304	5.14	3.69	0.19	2	7	3	264.237
ZINC12546012	4.43	4.28	1.74	2	4	3	272.26

From the ProTox 3.0® (Banerjee *et al.*, 2024) oral toxicity screening conducted, it was found that the toxicity of the molecules including the 3 highest affinity Lipinski Rule compliant molecules ranges from toxic if swallowed (Class 3) to potentially harmful if swallowed (Class 5). Toxicity results including the predicted toxicity class and predicted lethal dose 50 (LD_{50}) are summarised in Table 3.4.

Table 3.4: Predicted toxicity of the highest affinity Lipinski Rule compliant molecules, obtained from ProTox 3.0® (Banerjee *et al.*, 2024) (n=10).

ZINC Code	Predicted Toxicity Class	Predicted LD_{50} (mg/kg)	Cardiotoxicity	Carcinogenicity
ZINC48322609	4 – harmful if swallowed	1100	Inactive	Active
ZINC92968473	5 – may be harmful if swallowed	3500	Inactive	Inactive
ZINC00188045	3 – toxic if swallowed	300	Active	Inactive
ZINC94889747	4 – harmful if swallowed	2000	Active	Inactive
ZINC92203809	5 – may be harmful if swallowed	4000	Inactive	Active
ZINC19703382	4 – harmful if swallowed	800	Inactive	Active
ZINC56650139	5 – may be harmful if swallowed	3237	Active	Inactive
ZINC00188053	3 – toxic if swallowed	300	Active	Inactive
ZINC03985304	5 – may be harmful if swallowed	3000	Inactive	Inactive
ZINC12546012	4 – harmful if swallowed	1000	Inactive	Active

ZINC00188045 and ZINC48322609 as the highest affinity ZINC molecules were docked into the respective protomols and modelled in van der Waals radii in VMD® v1.9.3 (Humphrey *et al.*, 1996). The docked molecules are depicted in Figures 3.17 and 3.18 respectively.

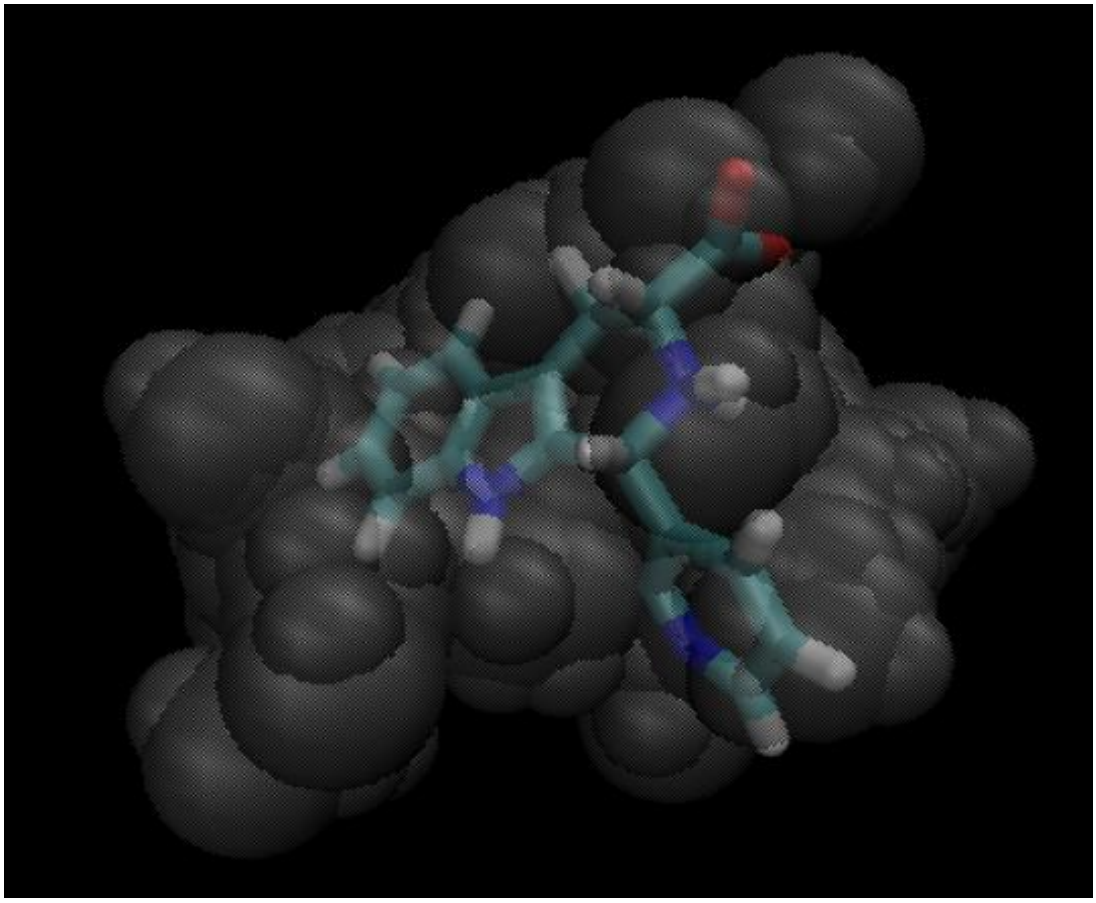

Figure 3.17: ZINC00188045, identified as the Lipinski Rule compliant molecule with the highest affinity to the PPARγ protomol with a binding affinity of 5.58, docked into the PPARγ protomol, as generated in VMD® v1.9.3 (Humphrey *et al.*, 1996).

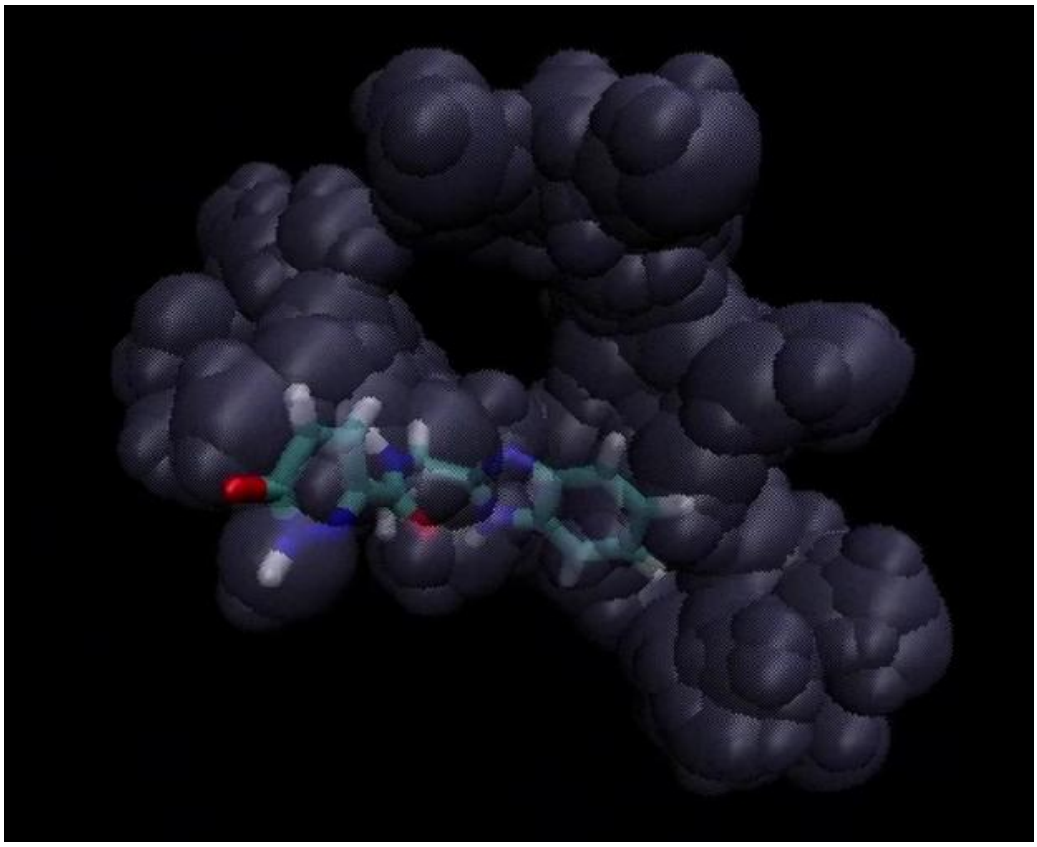

Figure 3.18: ZINC48322609, identified as the Lipinski Rule compliant molecule with the highest affinity to the ATR protomol with a binding affinity of 5.08, docked into the ATR protomol, as generated in VMD® v1.9.3 (Humphrey *et al.*, 1996).

3.2 *de Novo* Design Results

3.2.1 Optimal Conformer Identification

In the *de novo* design phase, the optimal conformation of HTR-04 (Chittiboyina *et al.*, 2009) for the PPARγ was modelled on the telmisartan scaffold while the optimal conformation of HTR-04 (Chittiboyina *et al.*, 2009) for the ATR was modelled on the olmesartan scaffold. The two conformations generated are depicted in Figures 3.19 and 3.20 respectively.

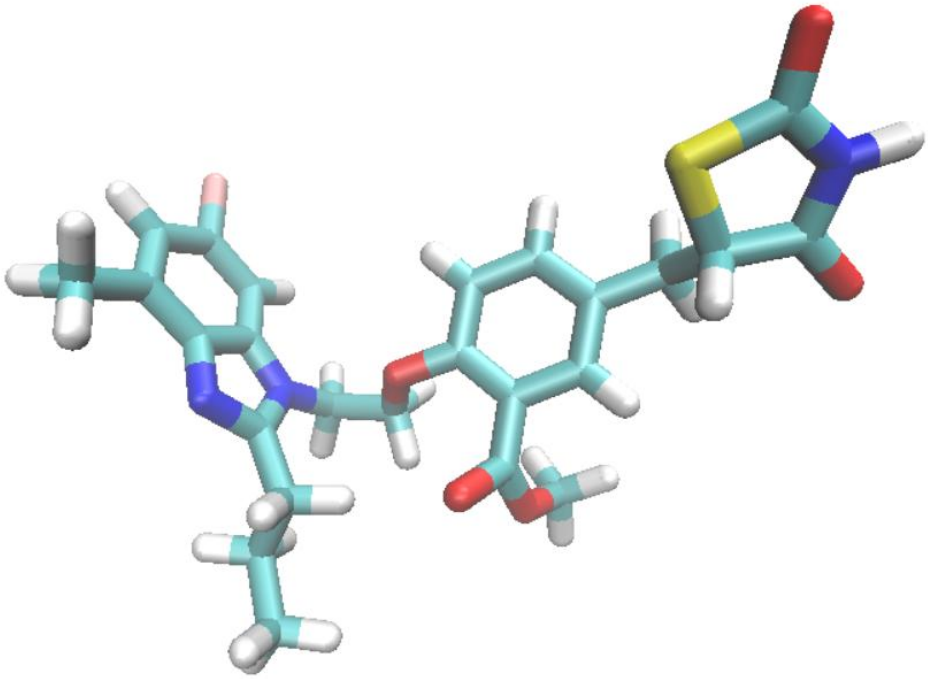

Figure 3.19: Optimal conformation of HTR-04 (Chittiboyina *et al.*, 2009) for the PPARγ as generated in VMD® v1.9.3 (Humphrey *et al.*, 1996).

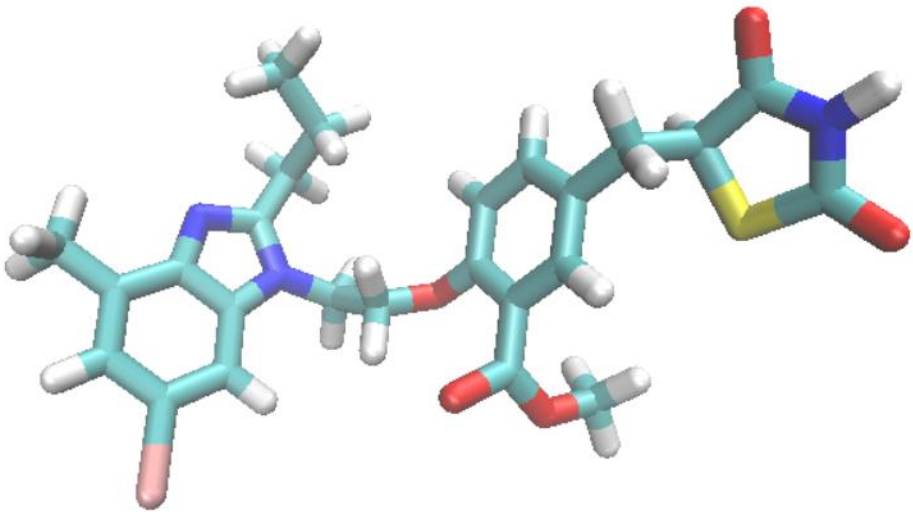

Figure 3.20: Optimal conformation of HTR-04 (Chittiboyina *et al.*, 2009) for the ATR as generated in VMD® v1.9.3 (Humphrey *et al.*, 1996).

3.2.2 Seed Structure Modelling

30 seed structures were designed in SYBYL-X® v1.1 (Ash *et al.*, 2010), 15 seed structures modelled for each of the two conformations of HTR-04 (Chittiboyina *et al.*, 2009), one conformer for the PPARγ and one conformer for the ATR. 10 seeds from each conformation were designed for molecular growth and 5 seeds from each conformation were designed for linkage. The 30 seed structures designed are depicted in Table 3.5. The interactions described in the generated 2D topology (Figures 3.21 and 3.22) maps guided the modelling of seed structures.

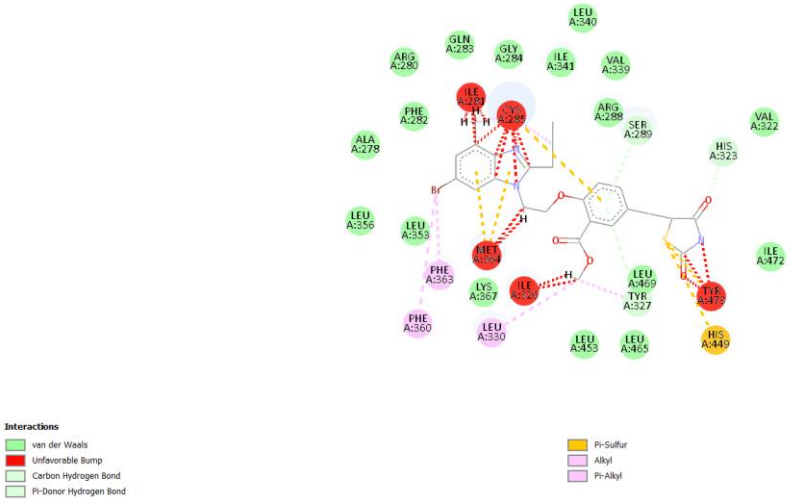

Figure 3.21: 2D topology map of the ligand-protein interactions between HTR-04 (Chittiboyina *et al.*, 2009) and PPARγ as described in PDB crystallographic deposition 3VN2[1], rendered in BIOVIA® Discovery Studio v24.1 (Baroroh *et al.*, 2023).

[1] Amano Y. RCSB PDB - 3VN2: Crystal structure of PPARgamma complexed with telmisartan [Internet]. United States: RCSB PDB. 2012 [cited 2025 Jul 4]. Available from: https://www.rcsb.org/structure/3VN2.

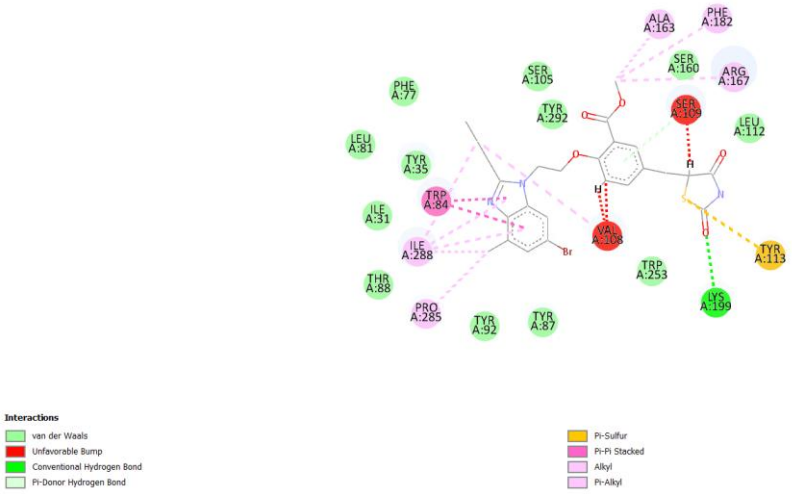

Figure 3.22: 2D topology map of the ligand-protein interactions between HTR-04 (Chittiboyina *et al.*, 2009) and ATR as described in PDB crystallographic deposition 4ZUD[2], rendered in BIOVIA® Discovery Studio v24.1 (Baroroh *et al.*, 2023).

[2] Zhang H, Unal H, Desnoyer R, Han GW, Patel N, Katritch V, *et al.* RCSB PDB - 4ZUD: Crystal structure of human angiotensin receptor in complex with inverse agonist olmesartan at 2.8Å resolution. [Internet]. United States: RCSB PDB. 2015 [cited 2025 Jul 4]. Available from: https://www.rcsb.org/structure/4ZUD.

Table 3.5: Seed structures designed in SYBYL-X® v1.1 (Ash *et al.*, 2010) for each of the two conformations of HTR-04 (Chittiboyina *et al.*, 2009), as rendered in VMD® v1.9.3 (Humphrey *et al.*, 1996).

'Grow' seeds within the PPARγ LBP	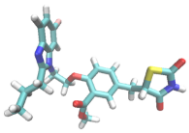	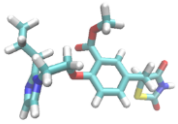	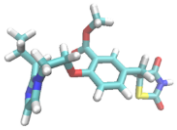	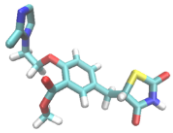	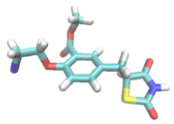
	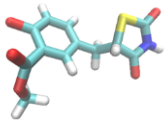	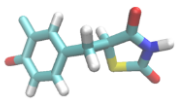	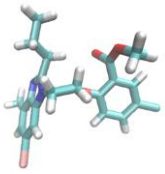	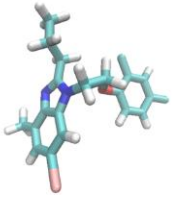	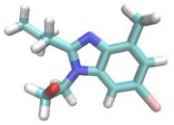
'Link' seeds within the PPARγ LBP	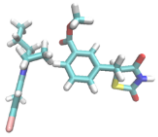	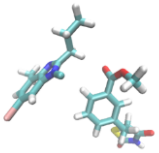	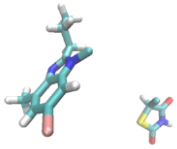	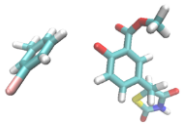	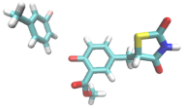
'Grow' seeds within the ATR LBP	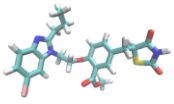	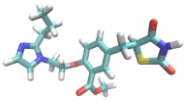	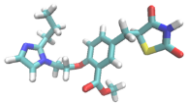	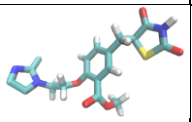	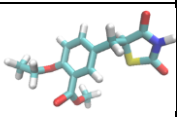
	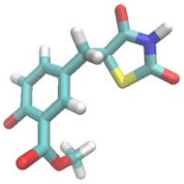	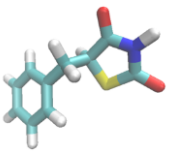	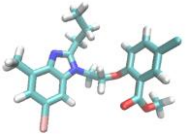	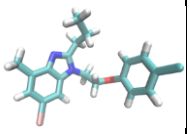	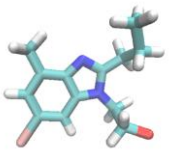
'Link' seeds within the ATR LBP	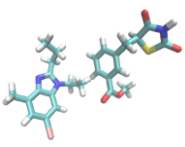	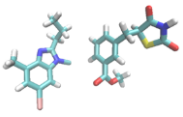	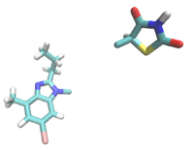	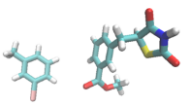	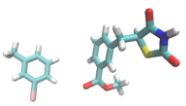

3.2.3 Ligand Binding Affinity Calculation

LBA (pKd) of the molecules bound to the target receptors PPARγ and ATR as obtained from their respective PDB crystallographic depositions was measured to establish a baseline affinity for comparison with molecules designed *de novo*, which should exhibit a greater affinity to the target receptors than the bound molecules. This process was carried out in X-SCORE® v1.3 (Wang *et al.*, 2002) where it was found that telmisartan exhibits a LBA (pKd) of 9.26 for the PPARγ as found in PDB crystallographic deposition 3VN2[1] and olmesartan exhibits a LBA (pKd) of 7.08 for the ATR as found in PDB crystallographic deposition 4ZUD[2].

[1] Amano Y. RCSB PDB - 3VN2: Crystal structure of PPARgamma complexed with telmisartan [Internet]. United States: RCSB PDB. 2012 [cited 2025 Jul 4]. Available from: https://www.rcsb.org/structure/3VN2.
[2] Zhang H, Unal H, Desnoyer R, Han GW, Patel N, Katritch V, *et al.* RCSB PDB - 4ZUD: Crystal structure of human angiotensin receptor in complex with inverse agonist olmesartan at 2.8Å resolution. [Internet]. United States: RCSB PDB. 2015 [cited 2025 Jul 4]. Available from: https://www.rcsb.org/structure/4ZUD.

3.2.4 Ligand Binding Pocket Modelling

The 'pharmacophore' and 'key site' files were produced when modelling receptor LBPs using the 'Pocket' module of LigBuilder® v1.2 (Yuan *et al.*, 2020).

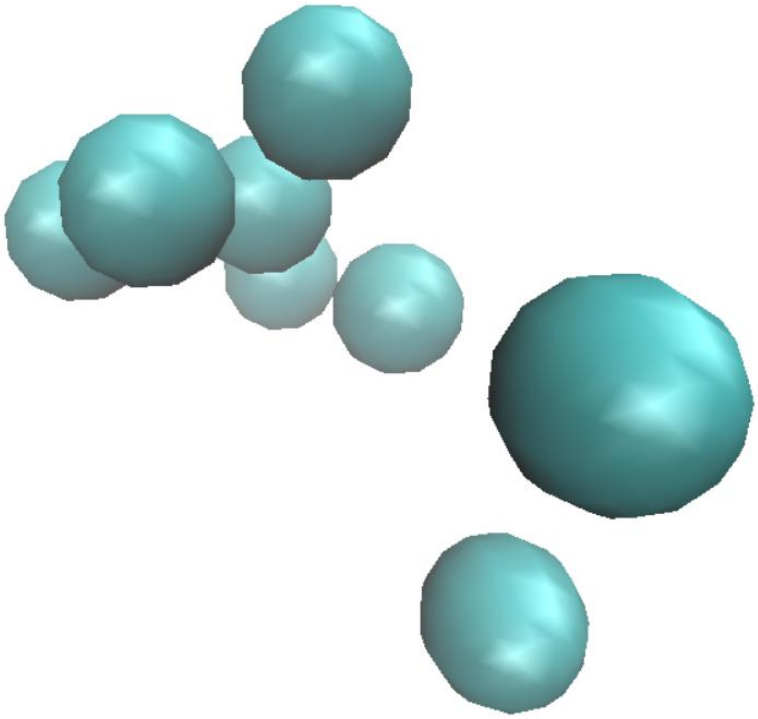

Figure 3.23: The telmisartan '*pharmacophor*e' generated in LigBuilder® v1.2 (Yuan *et al.*, 2020) based on the coordinates of PDB crystallographic deposition 3VN2[1] rendered in VMD® v1.9.3 (Humphrey *et al.*, 1996), depicting hydrophobic areas in green.

[1] Amano Y. RCSB PDB - 3VN2: Crystal structure of PPARgamma complexed with telmisartan [Internet]. United States: RCSB PDB. 2012 [cited 2025 Jul 4]. Available from: https://www.rcsb.org/structure/3VN2.

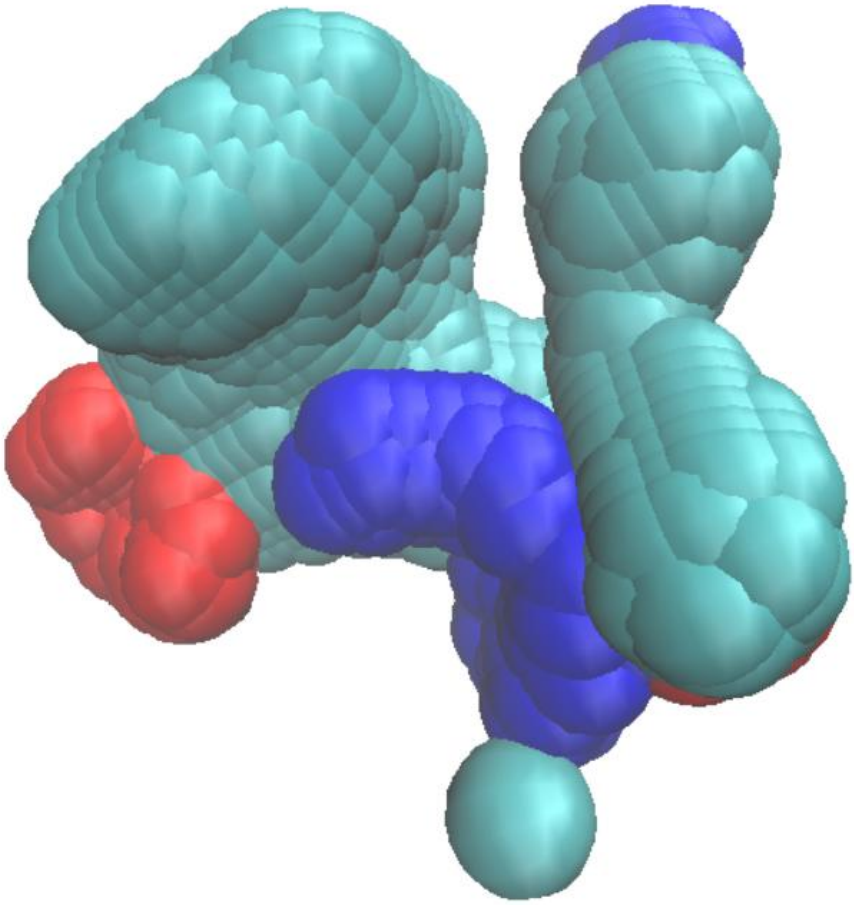

Figure 3.24: The telmisartan '*key site*' generated in LigBuilder® v1.2 (Yuan *et al.*, 2020) based on the coordinates of PDB crystallographic deposition 3VN2[1] rendered in VMD® v1.9.3 (Humphrey *et al.*, 1996), depicting HBD sites in blue, HBA sites in red and hydrophobic areas in green.

[1] Amano Y. RCSB PDB - 3VN2: Crystal structure of PPARgamma complexed with telmisartan [Internet]. United States: RCSB PDB. 2012 [cited 2025 Jul 4]. Available from: https://www.rcsb.org/structure/3VN2.

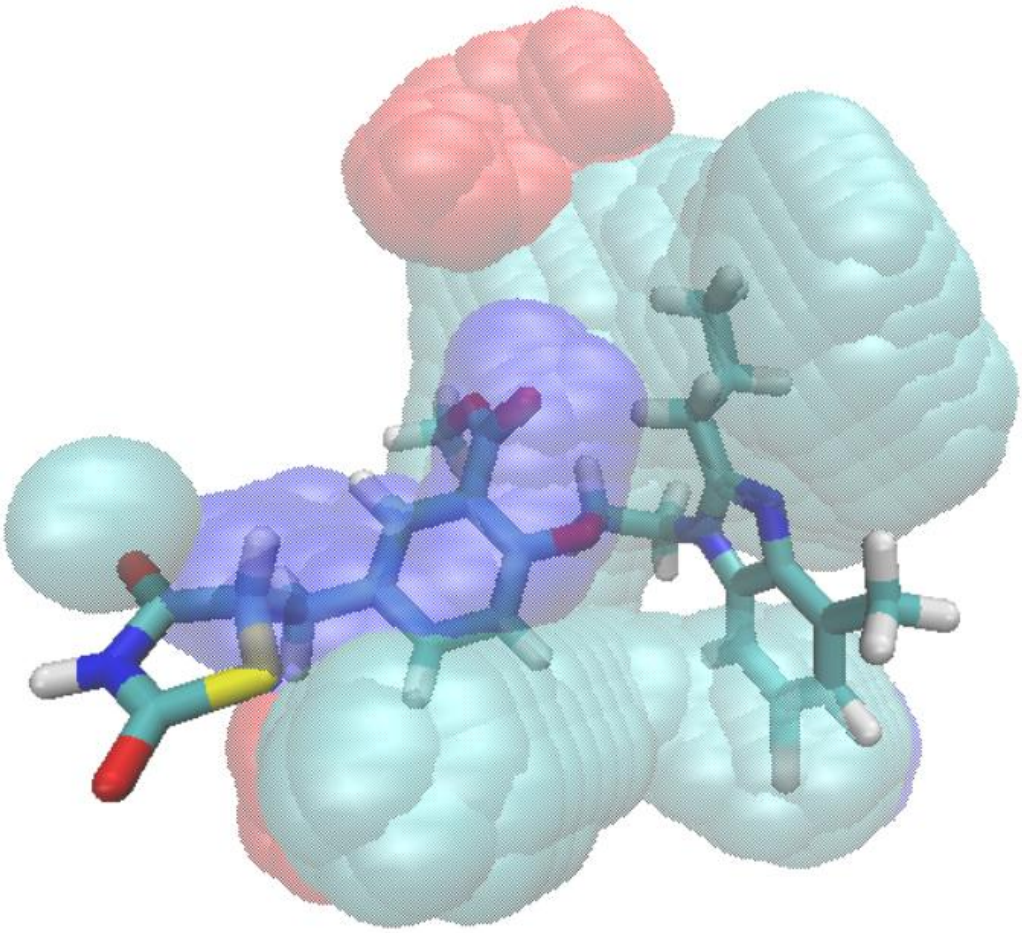

Figure 3.25: The optimal conformation of HTR-04 (Chittiboyina *et al.*, 2009) for the PPARγ embedded within the '*key site*' of the PPARγ, rendered in van der Waals radii in VMD® v1.9.3 (Humphrey *et al.*, 1996), depicting HBD sites in blue, HBA sites in red and hydrophobic areas in green.

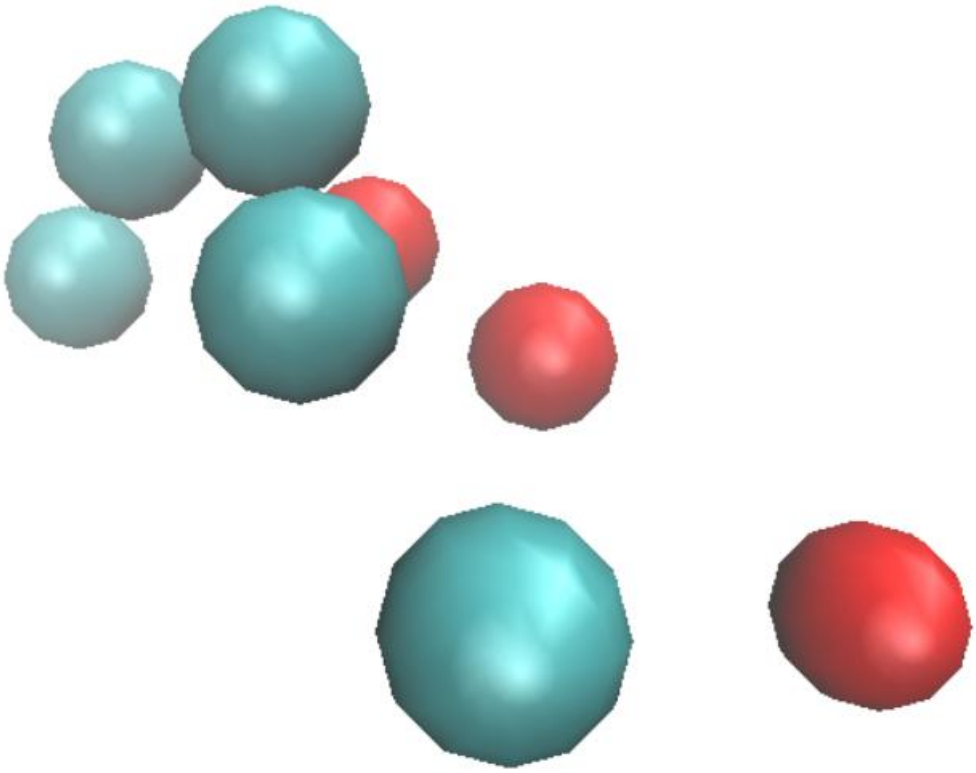

Figure 3.26: The olmesartan '*pharmacophor*e' generated in LigBuilder® v1.2 (Yuan *et al.*, 2020) based on the coordinates of PDB crystallographic deposition 4ZUD[2] rendered in VMD® v1.9.3 (Humphrey *et al.*, 1996), depicting HBA sites in red and hydrophobic areas in green.

[2] Zhang H, Unal H, Desnoyer R, Han GW, Patel N, Katritch V, *et al.* RCSB PDB - 4ZUD: Crystal structure of human angiotensin receptor in complex with inverse agonist olmesartan at 2.8Å resolution. [Internet]. United States: RCSB PDB. 2015 [cited 2025 Jul 4]. Available from: https://www.rcsb.org/structure/4ZUD.

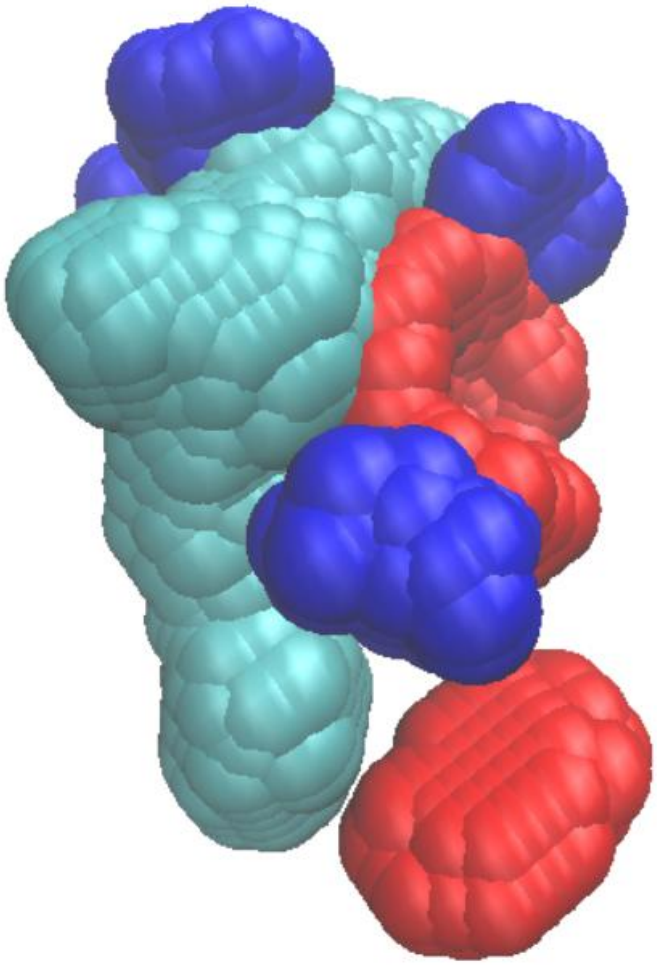

Figure 3.27: The olmesartan '*key site*' generated in LigBuilder® v1.2 (Yuan *et al.*, 2020) based on the coordinates of PDB crystallographic deposition 4ZUD[2] rendered in VMD® v1.9.3 (Humphrey *et al.*, 1996), depicting HBD sites in blue, HBA sites in red and hydrophobic areas in green.

[2] Zhang H, Unal H, Desnoyer R, Han GW, Patel N, Katritch V, *et al.* RCSB PDB - 4ZUD: Crystal structure of human angiotensin receptor in complex with inverse agonist olmesartan at 2.8Å resolution. [Internet]. United States: RCSB PDB. 2015 [cited 2025 Jul 4]. Available from: https://www.rcsb.org/structure/4ZUD.

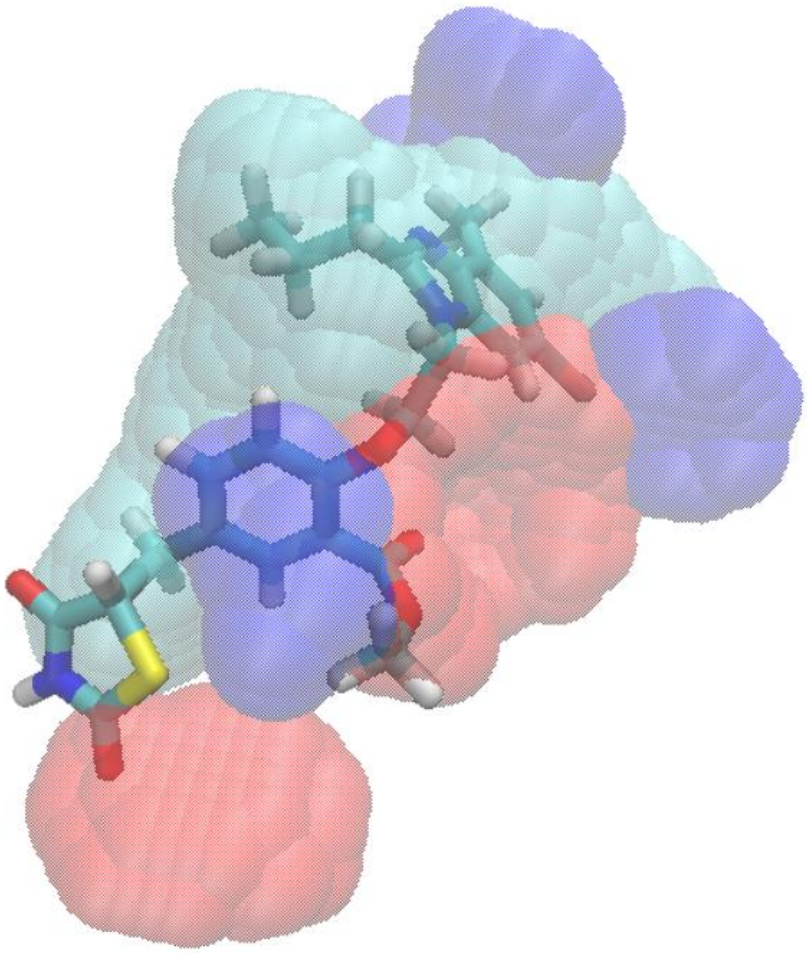

Figure 3.28 : The optimal conformation of HTR-04 (Chittiboyina *et al.*, 2009) for the ATR embedded within the '*key site*' of the ATR, rendered in van der Waals radii in VMD® v1.9.3 (Humphrey *et al.*, 1996), depicting HBD sites in blue, HBA sites in red and hydrophobic areas in green.

3.2.5 Identification of Highest-Affinity Molecules

Using the *de novo* design approach, 4132 molecules were generated from 1 successful seed. The seed structure is depicted in Figure 3.29 and was modelled from HTR-04 (Chittiboyina *et al.*, 2009) based on the ligand-protein interactions between HTR-04 (Chittiboyina *et al.*, 2009) and ATR as described in PDB crystallographic deposition 4ZUD.[2] Of the 4132 structures, the top 200 novel molecules were extracted into a molecular database on LigBuilder® v1.2 (Yuan *et al.*, 2020) after the 'Process' module was run. These novel molecules were derived from 17 molecular families as represented in Table 3.6.

Table 3.7 represents the physicochemical properties of the 10 highest affinity molecules generated from the seed (n=200) while Table 3.8 represents the binding scores of the structures for the PPARγ and ATR.

After filtration for Lipinski Rule compliance (Lipinski *et al.*, 2012), 3 molecules were found to be Lipinski Rule compliant, with none of these molecules being within the top 10 highest affinity molecules. The properties of these 3 molecules are tabulated in Tables 3.9 and 3.10.

From the ProTox 3.0® (Banerjee *et al.*, 2024) oral toxicity screening conducted, it was found that the toxicity of the molecules ranged from harmful if swallowed (Class 4) (n=9) to potentially harmful if swallowed (Class 5) (n=1). Toxicity results including the predicted toxicity class and predicted LD_{50} are summarised in Table 3.11.

[2] Zhang H, Unal H, Desnoyer R, Han GW, Patel N, Katritch V, *et al.* RCSB PDB - 4ZUD: Crystal structure of human angiotensin receptor in complex with inverse agonist olmesartan at 2.8Å resolution. [Internet]. United States: RCSB PDB. 2015 [cited 2025 Jul 4]. Available from: https://www.rcsb.org/structure/4ZUD.

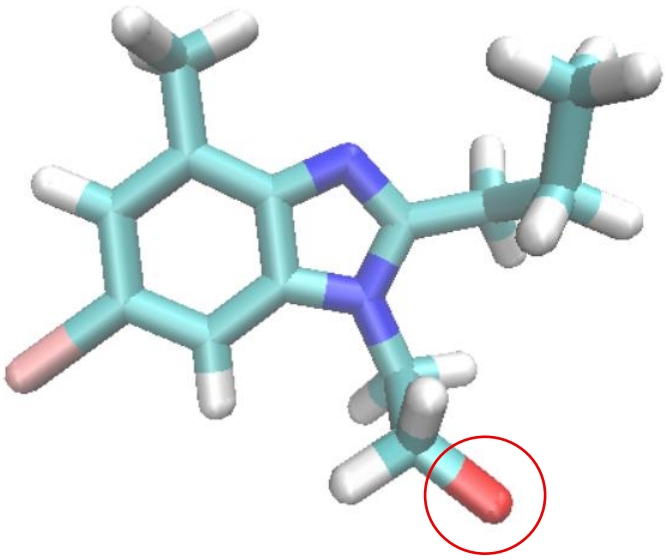

Figure 3.29: 3D structure of seed which sustained molecular growth, derived from HTR-04 (Chittiboyina *et al.,* 2009) based on the ligand-protein interactions between HTR-04 (Chittiboyina *et al.,* 2009) and ATR as described in PDB crystallographic deposition 4ZUD[2]. The atom circled in red denotes the special hydrogen atom at which molecular growth was sustained. Rendered in VMD® v1.9.3 (Humphrey *et al.*, 1996).

[2] Zhang H, Unal H, Desnoyer R, Han GW, Patel N, Katritch V, *et al.* RCSB PDB - 4ZUD: Crystal structure of human angiotensin receptor in complex with inverse agonist olmesartan at 2.8Å resolution. [Internet]. United States: RCSB PDB. 2015 [cited 2025 Jul 4]. Available from: https://www.rcsb.org/structure/4ZUD.

Table 3.6: Summary of molecules obtained from seed per family (N=200).

Molecular Family	Number of Molecules	Minimum pKd	Maximum pKd
1	111	8.61	9.99
2	10	8.62	9.97
3	7	8.61	9.90
4	3	8.81	9.77
5	11	8.65	9.76
6	7	8.75	9.74
7	29	8.64	9.46
8	1	9.15	9.15
9	5	8.70	9.13
10	3	8.66	9.07
11	4	8.64	8.99
12	1	8.97	8.97
13	4	8.74	8.90
14	1	8.90	8.90
15	1	8.87	8.87
16	1	8.79	8.79
17	1	8.77	8.77

Table 3.7: Physicochemical properties of the highest affinity molecules derived from *de novo* design (n=10).

Family	3D Molecular Structure	MW (Da)	cLogP	Chemical Score	HBDs	HBAs
1	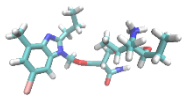	528	5.09	-120	3	5
1	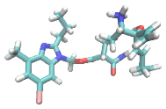	564	5.96	-100	3	5
2	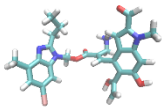	582	5.52	-60	3	5
1	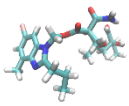	526	5.32	-100	2	6
1	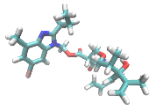	590	5.71	-100	2	6
1	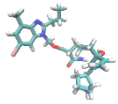	592	5.82	-120	3	5
3	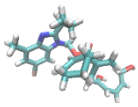	569	5.86	-70	2	4
1	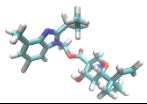	522	4.81	-160	2	5
1	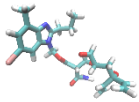	536	5.58	-110	2	6
1	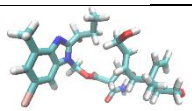	566	5.54	-100	3	6

Table 3.8: Binding score, expressed as a pKd of the highest affinity molecules derived from *de novo* design (n=10).

Family	3D Molecular Structure	PPARγ Binding Score (pKd)	ATR Binding Score (pKd)
1	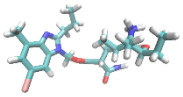	6.06	9.99
1	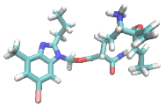	6.24	9.99
2	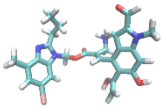	6.00	9.97
1	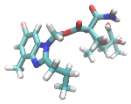	6.25	9.95
1	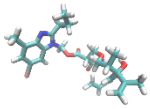	5.56	9.93
1	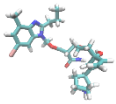	6.92	9.92
3	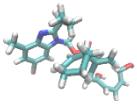	6.42	9.9
1	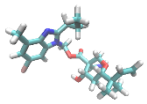	6.42	9.89
1	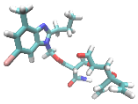	6.85	9.88
1	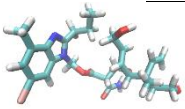	6.97	9.87

Table 3.9: Physicochemical properties of the Lipinski Rule compliant molecules derived from *de novo* design (n=3).

Family	3D Molecular Structure	MW (g/mol)	cLogP	Chemical Score	HBDs	HBAs
16	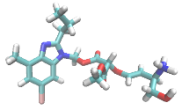	485	4.65	-100	2	5
1	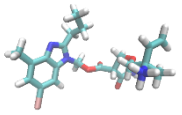	482	4.90	-80	2	4
1	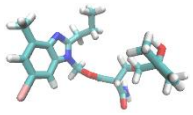	496	4.81	-80	2	5

Table 3.10: Binding score, expressed as a pKd of the highest affinity molecules derived from *de novo* design (n=3).

Family	3D Molecular Structure	PPARγ Binding Score (pKd)	ATR Binding Score (pKd)
16	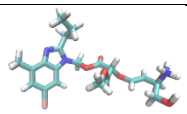	5.40	8.79
1	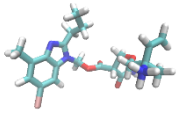	5.98	8.68
1	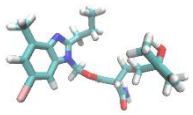	5.56	8.61

Table 3.11: Predicted toxicity of the highest-affinity structures, obtained from ProTOX-3.0® (Banerjee *et al.*, 2024) (n=10).

3D Molecular Structure	Predicted Toxicity Class	Predicted LD_{50} (mg/kg)	Cardiotoxicity	Carcinogenicity
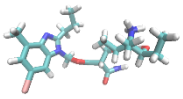	4 – harmful if swallowed	1000	Inactive	Inactive
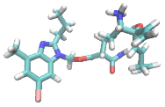	4 – harmful if swallowed	1105	Inactive	Inactive
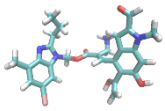	4 – harmful if swallowed	1743	Inactive	Inactive
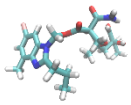	4 – harmful if swallowed	1105	Inactive	Inactive
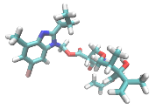	4 – harmful if swallowed	1743	Inactive	Inactive
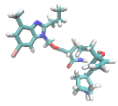	4 – harmful if swallowed	1105	Inactive	Inactive
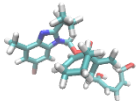	4 – harmful if swallowed	1743	Inactive	Inactive
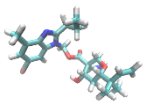	4 – harmful if swallowed	700	Inactive	Inactive
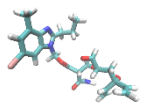	4 – harmful if swallowed	1105	Inactive	Inactive
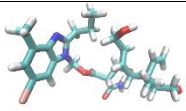	5 – may be harmful if swallowed	2500	Inactive	Inactive

Chapter 4

Discussion

4.1 Rationale of the Research

Rational drug design of an effective PPARγ modulator which maintains ATR antagonism of telmisartan would be ideal in the treatment of MetS. Such an agent could target several cardiovascular risk factors, reduce polypharmacy, adverse drug reactions and drug-drug interactions while optimising compliance and therapeutic outcomes (Lillich *et al.*, 2021).

As the ATR antagonist telmisartan is known to bind to, and act as an agonist at PPARγ (Schupp *et al.*, 2005; Imayama *et al.*, 2006; Gao *et al.*, 2018; Bernardo *et al.*, 2021; Wang *et al.*, 2022), the concept of dual PPARγ and ATR modulation becomes more relevant owing to the fact that dual agonists bearing the benzimidazole scaffold could, potentially, target the T2DM, dyslipidaemia, and hypertension characteristic of the highly prevalent MetS (Ellul & Shoemake, 2017, Lillich *et al.*, 2021).

The study identified a series of molecules which are both lead-like and capable of interaction with the PPARγ and the ATR. The optimal structures which will be further investigated and optimised are referred for molecular dynamic studies with the aim of identifying structures of simultaneous PPARγ agonism and ATR antagonism.

4.2 Virtual Screening Analysis

A total of 1468 hit molecules compliant with the Rule of Three (Congreve *et al.*, 2003) were identified using the ZINCPharmer® database (Koes & Camacho, 2012). These molecules exhibited considerable chemical and structural diversity and redundancy was possible since identical compounds may have been represented across multiple databases within the ZINCPharmer® chemical library. To address this, all 1468 molecules were subsequently filtered using MONA® (Hilbig & Rarey, 2015). which facilitated the removal of duplicate entries while simultaneously prioritising compounds with

favourable physicochemical characteristics. The refined set of molecules was then subjected to further evaluation in SYBYL-X® v1.1 (Ash *et al.*, 2010), where ranking was performed based on predicted binding affinity to receptor protomols, and in ProTOX-3.0® (Banerjee *et al.*, 2024), which enabled the investigation of predicted toxicity profiles.

All molecules were Lipinski rule (Lipinski *et al.*, 2012) compliant with respect to MW, with all molecules being less than 500Da. None of the molecules exceeded 5 HBDs or 10HBAs. CLogP values, a constant that predicts the partition coefficient and hence, the lipophilicity of the molecules, were within the range of 1-5 for the top 3 molecules, indicating a suitable lipophilicity for oral administration and intestinal absorption of the molecules. CLogP values for the remaining molecules fell below 1 (with the exception of ZINC00188053 and ZINC12546012), indicating poor lipophilicity and a greater hydrophilicity. CLogP values between 1-3 are even more favourable for orally administered drugs and for ideal intestinal absorption (Congreve *et al.*, 2003) with ZINC00188045, ZINC00188053, and ZINC12546012 all being suitable candidates that fall into this cLogP range.

4.2.1 Analysis of the Highest-Affinity Molecules

ZINC48322609, ZINC92968473 and ZINC00188045 were identified as the three molecules with the highest average affinity for the PPARγ and ATR protomols as identified from the 'Surflex-Dock' run carried out in SYBYL-X® v1.1 (Ash *et al.*, 2010).

ZINC48322609 exhibited the highest average affinity for both protomols with an average total score of 4.965 and the highest affinity for the ATR protomol with a total score of 5.08. It had a moderate MW of 282.283Da indicating a reasonable size for drug-likeness and a cLogP value of 2.38 which indicates moderate-high lipophilicity, predisposing to

adequate passive membrane permeability for oral administration and intestinal absorption paired with a balanced aqueous solubility (Lipinski *et al.*, 2012).

ZINC92968473 exhibited the second highest average affinity for both protomols with an average total score of 4.825. It had a moderate MW of 293.317 Da indicating a reasonable size for drug-likeness and a cLogP value of 3.29 which indicates increased lipophilicity, predisposing to increased membrane permeability for oral administration and intestinal absorption but lower water solubility (Lipinski *et al.*, 2012).

ZINC00188045 exhibited the third highest average affinity for both protomols with an average total score of 4.62 and the highest affinity for the PPARγ protomol with a total score of 5.58. It had a moderate MW of 293.326 Da indicating a reasonable size for drug-likeness and a cLogP value of 1.46 which indicates moderate-high hydrophilicity, predisposing to adequate water solubility and a moderate lipophilicity enabling membrane permeability for oral administration and intestinal absorption (Lipinski *et al.*, 2012).

From the ProTox 3.0® (Banerjee *et al.*, 2024) oral toxicity screening conducted, it was found that the toxicity of the molecules including the 3 highest affinity Lipinski Rule compliant molecules ranges from toxic if swallowed (Class 3) to potentially harmful if swallowed (Class 5). Only two molecules, ZINC92968473 and ZINC03985304, were predicted to be inactive when screened for cardiotoxicity and carcinogenicity with both molecules predicted to be of Class 5 toxicity. ZINC92968473 was found to be the least toxic of the ten highest-affinity molecules with a predicted LD_{50} of 3500mg/kg (Class 5) and no predicted cardiotoxicity or carcinogenicity. ZINC92203809 was found to have a higher predicted LD_{50} of 4000mg/kg (also Class 5), however it was predicted to be

actively cardiotoxic exhibited lower affinities for the protomols, ranking 5th based on its average total scores.

4.3 *de Novo* Design Analysis

Through the *de novo* design approach, 4,132 candidate molecules were generated from a single successful seed derived from HTR-04 (Chittiboyina *et al.*, 2009), which was modelled based on its interactions with the ATR as described in PDB crystallographic deposition 4ZUD.[2] From these, the top 200 structures, spanning 17 molecular families, were further evaluated as tabulated in Table 3.5. Analysis of the physicochemical properties of these structures (Table 3.6) highlighted some high-affinity candidates. However, only three molecules were compliant to Lipinski's Rule of Five (Lipinski *et al.*, 2012), and none of these structures ranked among the top 10 by binding affinity. This suggests that while the *de novo* design approach successfully generated diverse scaffolds with favourable binding potential, additional optimisation will be required to balance drug-likeness with affinity.

4.3.1 Analysis of the Highest-Affinity *de Novo* Structures

The 10 highest-affinity structures were all found to have a MW greater than 500Da, indicating reduced membrane permeability and absorption(Lipinski *et al.*, 2012). The structures also possess a cLogP greater than 5 indicating excessive lipophilicity which often leads to poor aqueous solubility, non-specific protein binding, and increased metabolic clearance. Simultaneously, these properties decrease the likelihood of

[2] Zhang H, Unal H, Desnoyer R, Han GW, Patel N, Katritch V, *et al.* RCSB PDB - 4ZUD: Crystal structure of human angiotensin receptor in complex with inverse agonist olmesartan at 2.8Å resolution. [Internet]. United States: RCSB PDB. 2015 [cited 2025 Jul 4]. Available from: https://www.rcsb.org/structure/4ZUD

achieving adequate systemic exposure following oral administration (Lipinski *et al.*, 2012). With respect to receptor binding affinity, all of the 10 highest-affinity structures exceeded the baseline LBA (pKd) for the ATR which was 7.08. This indicates that all structures bind to the ATR with a greater LBA than olmesartan, the inverse ATR agonist bound to the ATR as described in PDB crystallographic deposition 4ZUD[2], whose conformation was used to model the seed structure that sustained *de novo* molecular growth. When assessed for PPARγ affinity, the LBA (pKd) of the ARB and SPPARγM, telmisartan was utilised as a baseline LBA(pKd). This LBA(pKd) was found to be of 9.26. None of the 10 structures assessed for PPARγ affinity exhibited a LBA (pKd) greater than this baseline, indicating that although these structures may still bind to the PPARγ, however this binding is of a weaker nature than that exhibited by telmisartan. The difference in effective telmisartan concentrations for pharmacodynamic modulation of the PPARγ and ATR receptors is significant (Lillich *et al.*, 2021), suggesting that LBA (pKd) values greater than 9.26 are required for effective PPARγ modulation.

A total of 3 structures were found to be Lipinski-Rule compliant with MW values of 482Da, 485Da and, 496Da and cLogP values of 4.90, 4.65 and, 4.81 respectively. These values place the structures near the upper thresholds of the Rule of 5 by Lipinski *et al.* (2012). While the compounds are still within the acceptable limits for oral drug-likeness, they sit at the borderline where ADME challenges may begin to arise. Molecules of this size can still cross biological membranes, but permeability tends to decrease as molecular weight approaches 500 Da (Lipinski *et al.*, 2012). Similarly, cLogP values greater than 4 indicate relatively high lipophilicity, which can promote membrane permeability at the expense of aqueous solubility. Simultaneously, these properties suggest that such

[2] Zhang H, Unal H, Desnoyer R, Han GW, Patel N, Katritch V, *et al.* RCSB PDB - 4ZUD: Crystal structure of human angiotensin receptor in complex with inverse agonist olmesartan at 2.8Å resolution. [Internet]. United States: RCSB PDB. 2015 [cited 2025 Jul 4]. Available from: https://www.rcsb.org/structure/4ZUD.

compounds retain the potential for oral bioavailability but careful yet conservative optimisation of solubility is required to avoid pharmacokinetic liabilities (Lipinski *et al.*, 2012).

While none of these 3 molecules were amongst the 10 highest-affinity molecules for the ATR, they still possessed a LBA (pKd) for the ATR greater than that of olmesartan (7.08). Similarly to the 10 highest-affinity structures they also did not exhibit a LBA (pKd) for the PPARγ greater than that of telmisartan (9.26).

From the ProTox 3.0® (Banerjee *et al.*, 2024) oral toxicity screening conducted the 9 highest-affinity structures were predicted to be of Class 4 toxic (harmful if swallowed) with the 10th highest-affinity structure predicted to be of Class 5 toxicity (may be harmful if swallowed). Only two molecules, ZINC92968473 and ZINC03985304, were predicted to be inactive when screened for cardiotoxicity and carcinogenicity with both molecules predicted to be of Class 5 toxicity. ZINC92968473 was found to be the least toxic of the ten highest-affinity molecules with a predicted LD_{50} of 3500mg/kg (Class 5) and no predicted cardiotoxicity or carcinogenicity. ZINC92203809 was found to have a higher predicted LD_{50} of 4000mg/kg (also Class 5), however it was predicted to be actively cardiotoxic exhibited lower affinities for the protomols, ranking 5th based on its average total scores. All 10 structures were predicted to be inactive with respect to both cardiotoxicity and carcinogenicity.

4.4 The Virtual Screening & *de Novo* Approaches

VS has great benefits as an efficient, cost-effective, innovative and green rational drug design method. VS yields structurally-diverse molecules, especially when the query structure is a pharmacophore, as is the scenario in this project.

In this research, molecules obtained from VS were docked into protomols, energetically unsatisfied spaces at the core of target proteins. The methodology employed ensures an exhaustive exploration at the expense of uncertainty with respect to the bioactivity of the energetically active space as a whole. This may be addressed through a *de novo* fragment-based approach whereby molecules are docked into the active sites described in PDB crystallographic depositions which are known to be bioactive. The *de novo* fragment-based approach leads to a greater predisposition towards the bioactivity of the designed molecule but leaves a need for true structural innovation due to the close structural and pharmacological similarity of the generated molecules to the lead molecule of the study.

The primary objective of CADD is to employ VS strategies on large-scale chemical libraries and systematically identify promising hit and lead compounds. In addition to discovering novel scaffolds, CADD also enables the optimisation of pre-existing lead structures (Wu *et al.*, 2024). Through iterative refinement, this approach seeks to transform bioactive molecules into drug-like candidates by enhancing their physicochemical properties and improving critical physicochemical parameters, including ADME and toxicity, as well as overall pharmacokinetics (Wu *et al.*, 2024).

4.5 Limitations

Despite the relevant findings of this research and contributions to the understanding of potential dual PPARγ/ATR modulators, it is essential to acknowledge its inherent limitations. Chief among these is the reliance on *in silico* methodologies, which, despite their efficiency and predictive value, cannot fully replicate the multifaceted complexity of living biological systems, including dynamic biochemical and physiological interactions (Mihai & Nitulescu, 2025). The docking analyses were based on static

crystallographic structures that do not fully represent *in vivo* protein flexibility and dynamics (Mihai & Nitulescu, 2025). The results outlined in this study should be regarded as preliminary hypotheses rather than definitive conclusions. To ensure the robustness of these predictions, comprehensive experimental validation, through *in vitro* assays and *in vivo* models, is required to confirm the therapeutic efficacy and safety profile of the identified drug candidates.

Preferably, all of the 200 structures generated during the *de novo* design phase of the research would have been evaluated for their LBA for the PPARγ, with particular attention to those exhibiting a predicted LBA for the ATR greater than that of olmesartan. However, due to practical constraints, such comprehensive analysis could not be undertaken, which may have limited the identification of additional promising candidates with dual-target potential.

4.6 Further Studies & Recommendations

Future work should focus on validating these findings through *in vitro* assays, followed by *in vivo* evaluation of pharmacokinetics, efficacy, and safety. Molecular dynamics simulations and expansion of chemical space beyond benzimidazole derivatives are recommended to refine predictions and identify structurally diverse scaffolds. Comparative studies against established agents such as the ARB and SPPARγM telmisartan and the PPARγ agonist pioglitazone would also help benchmark the therapeutic potential of novel candidates.

4.7 Conclusion

This research applied CADD methodologies to identify and evaluate potential dual PPARγ/ATR modulators, employing hybrid benzimidazole scaffold to modulate structures that confer the dual pharmacological profile of telmisartan. Using pharmacophore modelling, VS, and *de novo* design, several candidate molecules were identified with promising binding affinities, acceptable physicochemical properties near the thresholds of drug-likeness, and favourable predicted toxicity profiles. Although these findings remain preliminary and require experimental validation, they provide a valuable framework for the rational development of novel therapeutics targeting metabolic and cardiovascular pathways. This work highlights the utility of *in silico* approaches in accelerating early-stage drug discovery and the potential of rational drug design to generate innovative dual PPARγ/ATR modulators, contributing towards more effective and simplified therapies for MetS.

References

Abbas A, Blandon J, Rude J, Elfar A, Mukherjee D. PPAR- γ agonist in treatment of diabetes: cardiovascular safety considerations. Cardiovascular & Hematological Agents in Medicinal Chemistry. 2012;10(2):124–34. doi: 10.2174/187152512800388948.

Abe M, Okada K, Kikuchi F, Matsumoto K. Clinical investigation of the effects of pioglitazone on the improvement of insulin resistance and blood pressure in type 2-diabetic patients undergoing hemodialysis. Clinical Nephrology. 2008;70(3):220–8. doi: 10.5414/cnp70220.

Alwhaibi M, Balkhi B, Alhawassi TM, Alkofide H, Alduhaim N, Alabdulali R, *et al.* Polypharmacy among patients with diabetes: a cross-sectional retrospective study in a tertiary hospital in Saudi Arabia. BMJ Open. 2018;8(5):e020852. doi: 10.1136/bmjopen-2017-020852.

Amano Y, Yamaguchi T, Ohno K, Niimi T, Orita M, Sakashita H, *et al.* Structural basis for telmisartan-mediated partial activation of PPAR gamma. Hypertension Research: Official Journal of the Japanese Society of Hypertension. 2012;35(7):715–9. doi: 10.1038/hr.2012.17.

Ash S, Cline MA, Homer RW, Hurst T, Smith GB. ChemInform Abstract: SYBYL Line Notation (SLN): A Versatile Language for Chemical Structure Representation. ChemInform. 2010; 28(18):66-78. doi: 10.1002/chin.199718282.

Attridge RL, Frei CR, Ryan L, Koeller J, Linn WD. Fenofibrate-associated nephrotoxicity: a review of current evidence. American Journal of Health-System Pharmacy. 2013;70(14):1219–25. doi: 10.2146/ajhp120131.

Bailey CJ, Kodack M. Patient adherence to medication requirements for therapy of type 2 diabetes. International Journal of Clinical Practice. 2011;65(3):314–22. doi: 10.1111/j.1742-1241.2010.02544.x.

Banerjee P, Kemmler E, Dunkel M, Preissner R. ProTox 3.0: a webserver for the prediction of toxicity of chemicals. Nucleic acids research. 2024;52(W1):W513–20. doi: 10.1093/nar/gkae303.

Baroroh U, Muscifa ZS, Destiarani W, Rohmatullah FG, Yusuf M. Molecular interaction analysis and visualization of protein-ligand docking using Biovia Discovery Studio Visualizer. Indonesian Journal of Computational Biology. 2023;2(1):22–30. doi: 10.24198/ijcb.v2i1.46322.

Benson SC, Pershadsingh HA, Ho CI, Chittiboyina A, Desai P, Pravenec M, *et al.* Identification of telmisartan as a unique angiotensin II receptor antagonist with selective PPARγ–modulating activity. Hypertension. 2004;43(5):993–1002. doi: 10.1161/01.hyp.0000123072.34629.57.

Bernardo A, Malara M, Bertuccini L, De Nuccio C, Visentin S, Minghetti L. The antihypertensive drug telmisartan protects oligodendrocytes from cholesterol accumulation and promotes differentiation by a PPAR-γ-mediated mechanism. International Journal of Molecular Sciences. 2021;22(17):9434. doi: 10.3390/ijms22179434.

Bernstein FC, Koetzle TF, Williams GJB, Meyer EF, Brice MD, Rodgers JR, *et al.* The Protein Data Bank: a computer-based archival file for macromolecular structures. Journal of Molecular Biology. 1977;112(3):535–42. doi: 10.1016/s0022-2836(77)80200-3.

Blundell TL, Jhoti H, Abell C. High-throughput crystallography for lead discovery in drug design. Nature Reviews Drug Discovery. 2002;1(1):45–54. doi: 10.1038/nrd706.

Chan SHH, Wu C-A, Wu KLH, Ho Y-H, Chang AYW, Chan JYH. Transcriptional upregulation of mitochondrial uncoupling protein 2 protects against oxidative stress-

associated 15 neurogenic hypertension. Circulation Research. 2009;105(9):886–96. doi: 10.1161/circresaha.109.199018.

Chittiboyina AG, Mizuno CS, Desai PV, Patny A, Kurtz TW, Pershadsingh HA, *et al.* Design, synthesis, and docking studies of novel telmisartan–glitazone hybrid analogs for the treatment of metabolic syndrome. Medicinal Chemistry Research. 2009;18(7):589–610. doi: 10.1007/s00044-008-9152-x.

Choo J, Yoon SJ, Ryu H, Park MS, Lee H, Park Y, *et al.* The Seoul Metropolitan Lifestyle Intervention Program and metabolic syndrome risk: a retrospective database study. International Journal of Environmental Research and Public Health. 2016;13(7):667. doi: 10.3390/ijerph13070667.

Congreve M, Carr R, Murray C, Jhoti H. A "Rule of Three" for fragment-based lead discovery?. Drug Discovery Today. 2003;8(19):876–7. doi: 10.1016/s1359-6446(03)02831-9.

Cross SS, Underwood JCE. Underwood's Pathology : a clinical approach. 7th ed. Edinburgh Churchill Livingstone, Elsevier; 2019.

Davis AM, Teague SJ, Kleywegt GJ. Application and limitations of X-ray crystallographic data in structure-based ligand and drug design. Angewandte Chemie International Edition. 2003;42(24):2718–36. doi: 10.1002/anie.200200539.

de Oliveira TA, da Silva MP, Maia Bechelane EH, da Silva AM, Gutterres Taranto A. Virtual Screening Algorithms in Drug Discovery: a Review Focused on Machine and Deep Learning Methods. Drugs Drug Candidates. 2023;2(2):311–34. doi: 10.3390/ddc2020017.

Derosa G, Ragonesi PD, Mugellini A, Ciccarelli L, Fogari R. Effects of telmisartan compared with eprosartan on blood pressure control, glucose metabolism and lipid profile in hypertensive, type 2 diabetic patients: a randomized, double-blind, placebo-controlled 12 month study. Hypertension Research. 2004;27(7):457–64. doi: 10.1291/hypres.27.457.

Dovinová I, Barancik M, Majzunova M, Zorad S, Gajdosechová L, Gresová L, *et al.* Effects of PPARγ agonist pioglitazone on redox-sensitive cellular signaling in young spontaneously hypertensive rats. PPAR Research. 2013;2013:1–11. doi: 10.1155/2013/541871.

Ellul C, Shoemake C. Design of novel compounds with the potential of dual PPARγ/α modulation for the management of metabolic syndrome. Nuclear Receptor Research. 2017;4. doi: 10.11131/2017/101311.

Gami AS, Witt BJ, Howard DE, Erwin PJ, Gami LA, Somers VK, *et al.* Metabolic syndrome and risk of incident cardiovascular events and death. Journal of the American College of Cardiology. 2007;49(4):403–14. doi: 10.1016/j.jacc.2006.09.032.

Gao Y, Li W, Liu Y, Wang Y, Zhang J, Li M, *et al.* Effect of telmisartan on preventing learning and memory deficits via peroxisome proliferator-activated receptor-γ in vascular dementia spontaneously hypertensive rats. Journal of Stroke and Cerebrovascular Diseases: The Official Journal of National Stroke Association. 2018;27(2):277–85. doi: 10.1016/j.jstrokecerebrovasdis.2017.01.025.

Golchin N, Isham L, Meropol S, Vince A, Frank S. Polypharmacy in the elderly. Journal of Research in Pharmacy Practice. 2015;4(2):85–8. doi: 10.4103/2279-042x.155755.

Grant RW, Devita NG, Singer DE, Meigs JB. Polypharmacy and medication adherence in patients with type 2 diabetes. Diabetes Care. 2003;26(5):1408–12. doi: 10.2337/diacare.26.5.1408.

Grundy SM, Cleeman JI, Daniels SR, Donato KA, Eckel RH, Franklin BA, *et al.* Diagnosis and management of the metabolic syndrome: an American Heart Association/National Heart, Lung, and Blood Institute scientific statement. Circulation. 2005;112(17):2735–52. doi: 10.1161/circulationaha.105.169404.

Grundy SM. Drug therapy of the metabolic syndrome: minimizing the emerging crisis in polypharmacy. Nature Reviews Drug Discovery. 2006;5(4):295–309. doi: 10.1038/nrd2005.

Guan Y, Hao C, Cha DR, Rao R, Lu W, Kohan DE, *et al.* Thiazolidinediones expand body fluid volume through PPARγ stimulation of ENaC-mediated renal salt absorption. Nature Medicine. 2005;11(8):861–6. doi: 10.1038/nm1278.

Hamada T, Kuwabara M, Watanabe A, Mizuta E, Ohtahara A, Omodani H, *et al.* A comparative study on the effectiveness of losartan/hydrochlorothiazide and telmisartan/hydrochlorothiazide in patients with hypertension. Clinical and Experimental Hypertension (New York, NY: 1993). 2014;36(4):251–7. doi: 10.3109/10641963.2013.810228.

Handelsman Y, Jellinger PS. Overcoming obstacles in risk factor management in type 2 diabetes mellitus. The Journal of Clinical Hypertension. 2011;13(8):613–20. doi: 10.1111/j.1751-7176.2011.00490.x.

Hilbig M, Rarey M. MONA 2: a Light Cheminformatics Platform for Interactive Compound Library Processing. Journal of Chemical Information and Modeling. 2015;55(10):2071–8. doi: 10.1021/acs.jcim.5b00292.

Humphrey W, Dalke A, Schulten K. VMD: Visual molecular dynamics. Journal of Molecular Graphics. 1996;14(1):33–8. doi: 10.1016/0263-7855(96)00018-5.

Imaizumi S, Miura S, Yahiro E, Uehara Y, Komuro I, Saku K. Class- and Molecule-specific Differential Effects of Angiotensin II Type 1 Receptor Blockers. Current Pharmaceutical Design. 2013;19(17):3002–8. doi: 10.2174/1381612811319170005.

Imayama I, Ichiki T, Inanaga K, Ohtsubo H, Fukuyama K, Ono H, *et al.* Telmisartan downregulates angiotensin II type 1 receptor through activation of peroxisome proliferator-activated receptor γ. Cardiovascular Research. 2006;72(1):184–90. doi: 10.1016/j.cardiores.2006.07.014.

Kirsch P, Hartman AM, Hirsch AKH, Empting M. Concepts and Core Principles of Fragment-Based Drug Design. Molecules. 2019;24(23):4309. doi: 10.3390/molecules24234309.

Koes DR, Camacho CJ. ZINCPharmer: Pharmacophore Search of the ZINC Database. Nucleic Acids Research. 2012; 40 (1): 409–414. doi: 10.1093/nar/gks378.

Kokubo Y, Okamura T, Yoshimasa Y, Miyamoto Y, Kawanishi K, Kotani Y, *et al.* Impact of metabolic syndrome components on the incidence of cardiovascular disease in a general urban Japanese population: the suita study. Hypertension Research: Official Journal of the Japanese Society of Hypertension. 2008;31(11):2027–35. doi: 10.1291/hypres.31.2027.

Kolli V, Stechschulte LA, Dowling AR, Rahman S, Czernik PJ, Lecka-Czernik B. Partial agonist, telmisartan, maintains PPARγ serine 112 phosphorylation, and does not affect osteoblast differentiation and bone mass. Marie PJ, editor. PLoS ONE. 2014;9(5):e96323. doi: 10.1371/journal.pone.0096323.

Kwak HJ, Pyun YM, Kim JY, Pagire HS, Kim KY, Kim KR, *et al.* Synthesis and biological evaluation of aminobenzimidazole derivatives with a phenylcyclohexyl acetic acid group as anti-obesity and anti-diabetic agents. Bioorganic & Medicinal Chemistry Letters. 2013;23(16):4713–8. doi: 10.1016/j.bmcl.2013.05.081.

Layne RD, Sehbai AS, Stark LJ. Rhabdomyolysis and Renal Failure Associated with Gemfibrozil Monotherapy. Annals of Pharmacotherapy. 2004;38(2):232–4. doi: 10.1345/aph.1d282.

Lillich FF, Imig JD, Proschak E. Multi-target approaches in metabolic syndrome. Frontiers in Pharmacology. 2021;11:554961. doi: 10.3389/fphar.2020.554961.

Lin Z, Sun L. Research advances in the therapy of metabolic syndrome. Frontiers in Pharmacology. 2024;15:1–26. doi:10.3389/fphar.2024.1364881.

Lipinski CA, Lombardo F, Dominy BW, Feeney PJ. Experimental and computational approaches to estimate solubility and permeability in drug discovery and development settings. Advanced Drug Delivery Reviews. 2012;64:4–17. doi: 10.1016/j.addr.2012.09.019.

Maertens A, Anastas N, Spencer PJ, Stephens M, Goldberg A, Hartung T. Green Toxicology. ALTEX. 2014;31(3):243–9. doi: 10.14573/altex.1406181.

Mihai DP, Nitulescu GM. Computer-Aided Drug Design and Drug Discovery. Pharmaceuticals. 2025;18(3):436–6. doi: 10.3390/ph18030436.

Miura S, Fujino M, Hanzawa H, Kiya Y, Imaizumi S, Matsuo Y, *et al.* Molecular mechanism underlying inverse agonist of angiotensin II type 1 receptor. The Journal of Biological Chemistry. 2006;281(28):19288–95. doi: 10.1074/jbc.M602144200.

Mottillo S, Filion KB, Genest J, Joseph L, Pilote L, Poirier P, *et al.* The metabolic syndrome and cardiovascular risk: a systematic review and meta-analysis. Journal of the American College of Cardiology. 2010;56(14):1113–32. doi: 10.1016/j.jacc.2010.05.034.

Naruse M, Koike Y, Kamei N, Sakamoto R, Yambe Y, Arimitsu M. Effects of azilsartan compared with telmisartan on insulin resistance in patients with essential hypertension and type 2 diabetes mellitus: An open-label, randomized clinical trial. Ngo DT, editor. PLoS One. 2019;14(4):e0214727. doi: 10.1371/journal.pone.0214727.

Nesto RW, Bell D, Bonow RO, Fonseca V, Grundy SM, Horton ES, *et al.* Thiazolidinedione Use, Fluid Retention, and Congestive Heart Failure: a Consensus Statement from the American Heart Association and American Diabetes Association: Response to Elasy and Griffin. Diabetes Care. 2004;27(8):256–63. doi: 10.2337/diacare.27.8.2096-a.

Nguyen JK, Fouts MM, Kotabe SE, Lo E. Polypharmacy as a risk factor for adverse drug reactions in geriatric nursing home residents. The American Journal of Geriatric Pharmacotherapy. 2006;4(1):36–41. doi: 10.1016/j.amjopharm.2006.03.002.

Nissen SE, Wolski K, Topol EJ. Effect of Muraglitazar on Death and Major Adverse Cardiovascular Events in Patients with Type 2 Diabetes Mellitus. JAMA. 2005;294(20):2581–6. doi: 10.1001/jama.294.20.joc50147.

Noale M, Veronese N, Perin PC, Pilotto A, Tiengo A, Crepaldi G, *et al.* Reply to letter to the editor "Polypharmacy in elderly people with diabetes admitted to hospital." Acta Diabetologica. 2016;53(5):859–60. doi: 10.1007/s00592-015-0819-8.

O'Toole MT, editor. Mosby's Medical Dictionary. 10th ed. Saint Louis, Missouri: Elsevier; 2017.

Pérez-Martínez P, Mikhailidis DP, Athyros VG, Bullo M, Couture P, Covas MI, *et al.* Lifestyle recommendations for the prevention and management of metabolic syndrome: an international panel recommendation. Nutrition Reviews. 2017;75(5):307–26. doi: 10.1093/nutrit/nux014.

Peterseim CM, Jabbour K, Mulki AK. Metabolic Syndrome: An Updated Review on Diagnosis and Treatment for Primary Care Clinicians. Journal of Primary Care & Community Health. 2024;15:1–11. doi:10.1177/21501319241309168.

Proschak E, Stark H, Merk D. Polypharmacology by Design: A Medicinal Chemist's Perspective on Multitargeting Compounds. Journal of Medicinal Chemistry. 2019;62(2):420–44. doi: 10.1021/acs.jmedchem.8b00760.

Rask Larsen J, Dima L, Correll CU, Manu P. The pharmacological management of metabolic syndrome. Expert Review of Clinical Pharmacology. 2018;11(4):397–410. doi: 10.1080/17512433.2018.1429910.

Ries UJ, Mihm G, Narr B, Hasselbach KM, Wittneben H, Entzeroth M, *et al.* 6-Substituted benzimidazoles as new nonpeptide angiotensin II receptor antagonists: synthesis, biological activity, and structure-activity relationships. Journal of Medicinal Chemistry. 1993;36(25):4040–51. doi: 10.1021/jm00077a007.

Rigamonti AE, Cicolini S, Tamini S, Caroli D, Cella SG, Sartorio A. The age-dependent increase of metabolic syndrome requires more extensive and aggressive non-pharmacological and pharmacological interventions: a cross-sectional study in an Italian cohort of obese women. Reimondo G, editor. International Journal of Endocrinology. 2021;2021:1–10. doi: 10.1155/2021/5576286.

Rodrigues MCS, De Oliveira C. Drug-drug interactions and adverse drug reactions in polypharmacy among older adults: an integrative review. Revista Latino-Americana de Enfermagem. 2016;24:e2800. doi: 10.1590/1518-8345.1316.2800.

Rollason V, Vogt N. Reduction of polypharmacy in the ederly. Drugs & Aging. 2003;20(11):817–32. doi: 10.2165/00002512-200320110-00003.

Schupp M, Clemenz M, Gineste R, Witt H, Janke J, Helleboid S, *et al.* Molecular characterization of new selective peroxisome proliferator-activated receptor gamma modulators with angiotensin receptor blocking activity. Diabetes. 2005;54(12):3442–52. doi: 10.2337/diabetes.54.12.3442.

Shindo T, Takasaki K, Uchida K, Onimura R, Kubota K, Uchida N, *et al.* Ameliorative effects of telmisartan on the inflammatory response and impaired spatial memory in a rat model of Alzheimer's disease incorporating additional cerebrovascular disease factors. Biological & Pharmaceutical Bulletin. 2012;35(12):2141–7. doi: 10.1248/bpb.b12-00387.

Stafylas PC, Sarafidis PA, Lasaridis AN. The controversial effects of thiazolidinediones on cardiovascular morbidity and mortality. International Journal of Cardiology. 2009;131(3):298–304. doi: 10.1016/j.ijcard.2008.06.005.

Sliwoski G, Kothiwale S, Meiler J, Lowe EW. Computational Methods in Drug Discovery. Pharmacological Reviews. 2013;66(1):334–95. doi: 10.1124/pr.112.007336.

Sun H. A Practical Guide to Rational Drug Design. Amsterdam: Elsevier/Woodhead Publishing; 2016.

Swinney DC, Anthony J. How were new medicines discovered? Nature Reviews Drug Discovery. 2011;10(7):507–19. doi: 10.1038/nrd3480

Tan Y, Muise ES, Dai H, Raubertas R, Wong KK, Thompson GM, *et al.* Novel transcriptome profiling analyses demonstrate that selective peroxisome proliferator-activated receptor γ (PPARγ) modulators display attenuated and selective gene regulatory activity in comparison with PPARγ full agonists. Molecular Pharmacology. 2012;82(1):68–79. doi: 10.1124/mol.111.076679.

Taskinen MR, Sullivan DR, Ehnholm C, Whiting M, Zannino D, Simes RJ, *et al.* Relationships of HDL Cholesterol, ApoA-I, and ApoA-II With Homocysteine and Creatinine in Patients With Type 2 Diabetes Treated With Fenofibrate. Arteriosclerosis Thrombosis and Vascular Biology. 2009;29(6):950–5. doi: 10.1161/atvbaha.108.178228.

Usuda D. Peroxisome proliferator-activated receptors for hypertension. World Journal of Cardiology. 2014;6(8):744. doi: 10.4330/wjc.v6.i8.744.

Viktil KK, Blix HS, Moger TA, Reikvam A. Polypharmacy as commonly defined is an indicator of limited value in the assessment of drug-related problems. British Journal of Clinical Pharmacology. 2007;63(2):187–95. doi: 10.1111/j.1365-2125.2006.02744.x.

Vitale C, Mercuro G, Castiglioni C, Cornoldi A, Tulli A, Fini M, *et al.* Metabolic effect of telmisartan and losartan in hypertensive patients with metabolic syndrome. Cardiovascular Diabetology. 2005;4(1):6. doi: 10.1186/1475-2840-4-6.

Wang R, Lai L, Wang S. Further development and validation of empirical scoring functions for structure-based binding affinity prediction. Journal of Computer-Aided Molecular Design. 2002;16(1):11–26. doi: 10.1023/a:1016357811882.

Wang HH, Lee DK, Liu M, Portincasa P, Wang DQH . Novel insights into the pathogenesis and management of the metabolic syndrome. Pediatric Gastroenterology, Hepatology & Nutrition. 2020;23(3):189. doi: 10.5223/pghn.2020.23.3.189.

Wang J, Pang T, Hafko R, Benicky J, Sanchez-Lemus E, Saavedra JM. Telmisartan ameliorates glutamate-induced neurotoxicity: Roles of AT1 receptor blockade and PPARγ activation. Neuropharmacology. 2014;79:249–61. doi: 10.1016/j.neuropharm.2013.11.022.

Wang R, Gao Y, Lai L. LigBuilder: a Multi-Purpose Program for Structure-Based Drug Design. Journal of Molecular Modeling. 2000;6(7-8):498–516. doi: 10.1007/s0089400060498.

Wang Y, Qiao S, Han DW, Rong XR, Wang YX, Xue J, *et al.* Telmisartan Improves Insulin Resistance. American Journal of Therapeutics. 2018;25(6):e642–51. doi: 10.1097/mjt.0000000000000733.

Wang Y, Zhang T, Li C, Guo J, Xu B, Xue L. Telmisartan attenuates human glioblastoma cells proliferation and oncogenicity by inducing the lipid oxidation. Asia-Pacific Journal of Clinical Oncology. 2022;18(3):217–23. doi: 10.1111/ajco.13574.

Wang ZZ, Shi XX, Huang GY, Hao G, Yang G. Fragment-based drug discovery supports drugging “undruggable” protein–protein interactions. Trends in Biochemical Sciences. 2023;48(6):539–52. doi: 10.1016/j.tibs.2023.01.008.

Willey CJ, Andrade SE, Cohen J, Fuller JC, Gurwitz JH. Polypharmacy with oral antidiabetic agents: an indicator of poor glycemic control. The American Journal of Managed Care. 2006;12(8):435–40.

Wolber G, Langer T. LigandScout: 3-D Pharmacophores Derived from Protein-Bound Ligands and their Use as Virtual Screening Filters. Journal of Computer-Aided Molecular Design. 2005; 45 (1): 160-169. doi: 10.1021/ci049885e.

Wu H, Liu J, Zhang R, Lu Y, Cui G, Cui Z, *et al.* A review of deep learning methods for ligand based drug virtual screening. Fundamental Research. 2024;4(4). doi: 10.1016/j.fmre.2024.02.011.

Wu Z, Chen S, Wang Y, Li F, Xu H, Li M, *et al.* Current perspectives and trend of computer-aided drug design: a review and bibliometric analysis. International Journal of Surgery. 2024;110(6):3848–78. doi: 10.1097/js9.0000000000001289.

Wüthrich K. The way to NMR structures of proteins. Nature Structural Biology. 2001;8(11):923–5. doi: 10.1038/nsb1101-923.

Yadav G, Ganguly S. Structure activity relationship (SAR) study of benzimidazole scaffold for different biological activities: A mini-review. European Journal of Medicinal Chemistry. 2015;97:419–43. doi: 10.1016/j.ejmech.2014.11.053.

Yang X, Wang Y, Byrne R, Schneider G, Yang S. Concepts of Artificial Intelligence for Computer-Assisted Drug Discovery. Chemical Reviews. 2019;119(18):10520–94. doi: 10.1021/acs.chemrev.8b00728.

Yu Y, Xue B-J, Wei S-G, Zhang Z-H, Beltz TG, Guo F, *et al.* Activation of central PPAR-γ attenuates angiotensin II-induced hypertension. Hypertension. 2015;66(2):403–11. doi: 10.1161/HYPERTENSIONAHA.115.05726.

Yuan Y, Pei J, Lai L. LigBuilder V3: a Multi-Target *de Novo* Drug Design Approach. Frontiers in Chemistry. 2020;8:1–18. doi: 10.3389/fchem.2020.00142.

Zhang F, Lavan BE, Gregoire FM. Selective modulators of PPAR-γ activity: molecular aspects related to obesity and side-effects. PPAR Research. 2007;2007:1–7. doi: 10.1155/2007/32696.

Zhang H, Unal H, Desnoyer R, Han GW, Patel N, Katritch V, *et al.* Structural Basis for Ligand Recognition and Functional Selectivity at Angiotensin Receptor. Journal of Biological Chemistry. 2015;290(49):29127–39. doi: 10.1074/jbc.m115.689000.

Zhou H, Cao H, Skolnick J. FRAGSITE: a Fragment-Based Approach for Virtual Ligand Screening. Journal of Chemical Information and Modeling. 2021;61(4):2074–89. doi: 10.1021/acs.jcim.0c01160.

List of Publications

The following poster was submitted for the 83rd International Pharmacy Federation (FIP) World Congress of Pharmacy and Pharmaceutical Sciences (FIP Copenhagen 2025).

L-Università ta' Malta | Faculty of Medicine & Surgery | Department of Pharmacy

Design and Optimisation of Novel Benzimidazole Hybrid Structures Capable of Simultaneous Peroxisome Proliferator Activated Receptor γ (PPARγ) and Angiotensin Receptor (ATR) Modulation

Matthias Borg[1], Dr. Claire Shoemake[1]

[1]Department of Pharmacy, Faculty of Medicine and Surgery, University of Malta, Msida, Malta

email: matthias.borg.20@um.edu.mt

INTRODUCTION

Metabolic syndrome (MetS) has serious clinical implications and is linked to an increased predisposition to diabetes mellitus and cardiovascular disease.

Polypharmacy, prevalent in the current management of MetS, is often inadequate in disease management.

Literature indicates that dual PPARγ/ATR modulators have potential in the management of MetS.[1]

AIM

To use the binding interactions of the benzimidazole scaffold with both PPARγ and ATR receptors to model structures with simultaneous high affinity for both ligand binding pockets using virtual screening and *de novo* design approaches.

METHOD

Virtual Screening

- PDB crystallographic depositions 3VN2[2] and 4ZUD[3] identified from Protein Data Bank
- Benzimidazole structure, HTR-04[4] identified from literature & modelled in SYBYL-X®
- Binding interactions of HTR-04[4], telmisartan & olmesartan used to build shared-feature (consensus) pharmacophore
- ZINCPharmer® database queried using the modelled consensus pharmacophore
- PPARg and ATR protomols modelled in SYBYL-X® and hits filtered for Rule of 3 compliance docked
- Toxicity screening performed in ProTOX-3.0®

de Novo Design

- 2D topology maps describing the critical interactions between HTR-04[4] and PPARγ and ATR generated
- Seed structures modelled from HTR-04[4] based on 2D topology maps
- 3D model of receptor ligand binding pockets created
- Seed structures docked into receptor ligand binding pocket for molecular growth
- Highest-ranking Lipinski Rule compliant novel molecules identified

RESULTS

Virtual Screening

- 1468 hit molecules
- 519 Lipinski-Rule compliant lead molecules

Table 1: Physicochemical properties of the 3 highest affinity Lipinski Rule compliant molecules.

Molecular Structure	PPARγ Affinity (Total Score)	ATR Affinity (Total Score)	cLogP	H-Bond Donors	H-Bond Acceptors	Rotatable Bonds	Molecular Weight (g/mol)	Predicted LD50 (mg/kg)
	4.85	5.08	2.38	2	5	4	282.283	1100
	5.04	4.61	3.29	1	1	3	293.317	3500
	5.58	3.66	1.46	2	2	2	293.326	300

de Novo Design

- 4132 molecules generated from 1 seed structure derived from HTR-04[4] based on the ligand-protein interactions between HTR-04[4] and ATR

Table 2: Physicochemical properties of the 3 highest affinity molecules derived from *de novo* design.

Molecular Structure	Molecular Weight (g/mol)	cLogP	Binding Score (pKd)	Chemical Score	H-Bond Donors	H-Bond Acceptors
	528	5.09	9.99	-120	3	5
	564	5.96	9.99	-100	3	5
	582	5.52	9.97	-60	3	5

CONCLUSION

Rational drug design of an effective PPARγ modulator which maintains ATR antagonism of telmisartan would be ideal in the treatment of MetS. Such an agent can target several cardiovascular risk factors, reduce polypharmacy, adverse drug reactions and drug-drug interactions while optimising compliance and therapeutic outcomes. Virtual screening is an efficient, cost-effective, and green drug design method that yields structurally diverse molecules at the expense of uncertainty with respect to the bioactivity of the energetically active space as a whole. Using a *de novo* fragment-based approach with known bioactive sites improves bioactivity prediction but limits structural innovation due to similarity with the lead compound.

REFERENCES

1. Peterseim CM, Jabbour K, Mulki AK. Metabolic Syndrome: An Updated Review on Diagnosis and Treatment for Primary Care Clinicians. Journal of Primary Care & Community Health. 2024;15:1–11. doi:10.1177/21501319241309168.
2. Amano Y. RCSB PDB - 3VN2: Crystal structure of PPARgamma complexed with telmisartan [Internet]. United States: RCSB PDB. 2012 [cited 2025 May 14]. Available from: https://www.rcsb.org/structure/3VN2.
3. Zhang H, Unal H, Desnoyer R, Han GW, Patel N, Katritch V, et al. RCSB PDB - 4ZUD: Crystal structure of human angiotensin receptor in complex with inverse agonist olmesartan at 2.8Å resolution. [Internet]. United States: RCSB PDB. 2015 [cited 2025 May 14]. Available from: https://www.rcsb.org/structure/4ZUD.
4. Chittiboyina AG, Mizuno CS, Desai PV, Patny A, Kurtz TW, Pershadsingh HA, et al. Design, synthesis, and docking studies of novel telmisartan–glitazone hybrid analogs for the treatment of metabolic syndrome. Medicinal Chemistry Research. 2009;18(7):589–610. doi: 10.1007/s00044-008-9152-x.

Appendix 1

The status of your REDP form (MED-2024-00115) has been updated to Acknowledged

Inbox ×

form.urec@um.edu.mt Mon, 22 Apr, 07:58

to me

Dear Matthias Borg,

Please note that the status of your REDP form (MED-2024-00115) has been set to *Acknowledged*.

This status change was accompanied by the following explanation/justification: *Dear applicant, Your research ethics application has been received. This does not mean that your application has FREC ethical approval and may be subject to an audit review. The FREC number generated by submission for records only cannot be used as proof of ethical approval. As indicated in the Research Ethics Review Procedures, submissions which have no self-assessment issues are kept for record and audit purposes only, so research may commence. Kindly note that FREC will not issue any form of approval as the responsibility for the self-assessment part lies exclusively with the researcher. Please note that SCPD generally requires review. If you have any questions or doubts or require any further clarification you can contact the MED FREC secretary. Regards, MED FREC*